Studies of the Relative Biological Effectiveness and Biological Dose in Proton and Carbon Ion Therapy

Tordis Johnsen Dahle

Thesis for the degree of Philosophiae Doctor (PhD)
University of Bergen, Norway
2020

UNIVERSITY OF BERGEN

Studies of the Relative Biological Effectiveness and Biological Dose in Proton and Carbon Ion Therapy

Tordis Johnsen Dahle

Thesis for the degree of Philosophiae Doctor (PhD)
at the University of Bergen

Date of defense: 28.04.2020

Year: 2020

Title: Studies of the Relative Biological Effectiveness and Biological Dose in Proton and Carbon Ion Therapy

Name: Tordis Johnsen Dahle

Print: Skipnes Kommunikasjon / University of Bergen

Scientific environment

The work in this thesis has been a part of the project “3D microdosimetry and studies of the Relative Biological Effectiveness (RBE) in proton- and carbon therapy”, funded by the Trond Mohn Foundation and the University of Bergen. The project is organized by project leader Kristian Smeland Ytre-Hauge within the subatomic physics group at the Department of Physics and Technology, University of Bergen.

The PhD project has been conducted in close collaboration with Monte Carlo experts at Centro Nazionale di Adroterapia Oncologica (CNAO) in Italy, and with the group for Biophysics and Medical Physics at the University of Oslo. The work in this PhD has also been aided by researchers/experts within radiation therapy and general medical physics at the Department of Oncology and Medical Physics at Haukeland University Hospital.

Supervisors

Kristian Smeland Ytre-Hauge
Department of Physics and Technology, University of Bergen, Norway

Andrea Mairani
Heidelberg Ion-beam Therapy Center (HIT), Germany
Centro Nazionale di Adroterapia Oncologica (CNAO), Italy

Camilla Hanquist Stokkevåg
Department of Oncology and Medical Physics, Haukeland University Hospital, Norway
Department of Physics and Technology, University of Bergen, Norway

Evaluation committee

Armin Lühr
OncoRay – National Center for Radiation Research in Oncology, Dresden, Germany
Faculty of Physics, TU Dortmund University, Germany

Brita Singers Sørensen
Department of Experimental Clinical Oncology and Danish Center for Particle Therapy, Aarhus University Hospital, Denmark

Martin Møller Greve
Department of Physics and Technology, University of Bergen, Norway

Acknowledgements

This thesis could not have been written without help and support from the people I have worked with the last four years. I am very grateful and privileged for the opportunity this thesis has given me to work with all of you. The thesis would neither have been possible without funding. I am grateful for the financial support from the University of Bergen and the Trond Mohn Foundation.

However, I would first and foremost like to thank my main supervisor, Kristian Smeland Ytre-Hauge, for all the help and encouragement throughout these years. Thank you for giving me this opportunity and for guiding me through these four years. Your support in all parts of this PhD project has been invaluable. I really appreciate all the time you spend on making your group in medical physics into such a good place to be.

I want to give warm thanks to my co-supervisors Andrea Mairani and Camilla Stokkevåg. Thank you, Andrea, for inviting me to spend five weeks at CNAO in Pavia. Our discussions and your help with FLUKA have been very valuable. I really appreciate that you always have been available, also after my stay in Pavia. To Camilla: Thank you for your guidance during these years. I really appreciate your clinical insight and all the work you have put into helping me, especially by giving positive and constructive feedback on my work.

My stay at CNAO gave me a more practical insight to the field of particle therapy, and I got to know many people who helped me with my work. Thanks to Giuseppe Magro, for welcoming me to CNAO and making sure that I had a good time both at and after work. Your help, both at CNAO and later, has really been appreciated. I would also like to thank Kyungdon Choi for help with programming during and after my stay at CNAO.

I would like to acknowledge all my collaborators in Oslo. I am especially grateful to Eirik Malinen, who has been my main contact there and who has been involved in all my work with the Oslo group. I would also like to thank Nina Edin and Anne Marit Rykkelid for giving me insight into cell irradiation experiments and for help on the Oslo Cyclotron Laboratory beamline, and Espen Rusten for help with the hypoxia project, especially with analyzing PET images. Through the people in Oslo, I was also introduced to several PET experts in Turku, Finland, and I would like to thank you all for sharing your knowledge.

The work in this thesis has been done in close collaboration with people at the Department of Oncology and Medical Physics at Haukeland University Hospital. I would like to thank you all for help on dose planning and clinical insight, especially Camilla Grindeland Boer, Liv Hysing, Ellen Marie Høye and Sara Pilskog.

I would like to thank all my friends at IFT. Eivind Rørvik, Lars Fredrik Fjæra, Andreas Tefre Samnøy and Helge Henjum, thank you for all the fruitful discussions and help. Together with Lucas, Ingrid and Renate, you have made my lunch breaks and years as a PhD student more sociable and enjoyable.

At last, but not least, I would like to thank my family and friends, for your encouragement and support these last four years. You really mean a lot to me.

Abstract

Protons and heavier ions have an increased relative biological effectiveness (RBE) compared to photons. While variable RBE models are applied clinically in carbon ion therapy, the RBE in proton therapy is accounted for clinically by applying a constant RBE of 1.1. However, an increasing amount of experimental and clinical data show that also the proton RBE varies spatially within the patient. In addition, the existing carbon ion RBE models give substantially different RBE-weighted dose (often referred to as biological dose) distributions for the same irradiation scenarios. Improving the current RBE calculations is therefore crucial for the treatment received by patients. In this thesis, variables affecting the RBE and biological dose models were studied using the FLUKA Monte Carlo code.

In the first part of the thesis, a low-energy proton beam cell irradiation experiment at the Oslo Cyclotron Laboratory (OCL) was implemented in FLUKA (Paper I). Applying the FLUKA implementation, the dose and linear energy transfer (LET) (both the dose-averaged LET (LET_d) and LET spectra) were estimated in potential cell irradiation positions. The LET_d values increased along the beam path, up to approximately 40 keV/µm in the distal dose-fall off. The LET spectra became narrower with depth in water. Comparisons with a simulated 80 MeV proton beam showed that the OCL beam had significantly higher LET_d values and much narrower LET spectra for the same LET_d values. The FLUKA implementation of the OCL beam demonstrated the importance of having proper proton beam characteristics to achieve accurate RBE versus LET data.

In the second part of the thesis, the RBE model applied clinically in carbon ion therapy in Japan (the microdosimetric kinetic model, MKM) was implemented in FLUKA (Paper II). For the implementation, tables connecting the saturation-corrected dose-mean specific energy (z_{1D}^*) to particle type and particle kinetic energy were generated. The FLUKA implementation was then used to study the sensitivity of the MKM to variations in the model parameters (Paper III). The created z_{1D}^* tables agreed well with the tables applied clinically in Japan. The

relative changes in the biological dose distributions during the sensitivity study were less than the percentage change of a model parameter. In addition, varying multiple parameters simultaneously had mostly smaller impact on the biological dose than varying parameters separately. The MKM implementation enables conversion from dose distributions obtained with the local effect model (European RBE model) to MKM dose distributions, making direct comparisons to the Japanese clinical carbon ion data possible.

In the final part of the thesis, a biological dose model accounting for hypoxia was developed for protons and implemented in FLUKA (Paper IV), as well as in a FLUKA based treatment planning tool (Paper V). The hypoxia model estimates the biological dose as a function of RBE and oxygen enhancement ratio (OER). The OER is a function of the LET and the partial oxygen pressure (pO_2), which was estimated in patients using [^{18}F]-EF5 PET images. Areas with low pO_2 values were observed in the planning target volume of a head and neck cancer patient, resulting in volumes of lower biological dose than prescribed. Treatment plans optimized with the hypoxia method had a median biological dose corresponded with the prescription dose and physical dose distributions which were increased in the hypoxic areas. The optimization of treatment plans with the hypoxic model showed good potential for including the OER, as well as the RBE, in treatment planning.

Overall, this thesis has contributed to knowledge on the RBE and biological dose calculations in proton and carbon ion therapy. Monte Carlo studies of an experimental or clinical proton or carbon ion beam may help reducing the uncertainties in the RBE and biological dose. Given the increase in proton and carbon ion facilities worldwide, improving the accuracy of RBE calculations to give patients the best possible treatment is more relevant than ever.

List of publications

Paper I **Dahle TJ**, Rykkelid AM, Stokkevåg CH, Mairani A, Görgen A, Edin NJ, Rørvik E, Fjæra LF, Malinen E, Ytre-Hauge KS (2017). *Monte Carlo simulations of a low energy proton beamline for radiobiological experiments*. Acta Oncologica, 56(6), 779-786.

Paper II Magro G**, Dahle TJ**, Molinelli S, Ciocca M, Fossati P, Ferrari A, Inaniwa T, Matsufuji N, Ytre-Hauge KS, Mairani A (2017). *The FLUKA Monte Carlo code coupled with the NIRS approach for clinical dose calculations in carbon ion therapy*. Physics in Medicine & Biology, 62, 3814.

Paper III **Dahle TJ**, Magro G, Ytre-Hauge KS, Stokkevåg CH, Choi K, Mairani A (2018). *Sensitivity study of the microdosimetric kinetic model parameters for carbon ion radiotherapy*. Physics in Medicine & Biology, 63, 225016.

Paper IV **Dahle TJ**, Rusten E, Stokkevåg CH, Silvoniemi A, Mairani A, Fjæra LF, Rørvik E, Henjum H, Wright P, Boer CG, Forsback S, Minn H, Malinen E, Ytre-Hauge KS. *The FLUKA Monte Carlo code coupled with a hypoxia model for biological dose calculations in proton therapy.* (Submitted to Physica Medica).

Paper V **Dahle TJ**, Henjum H, Mairani A, Stokkevåg CH, Boer CG, Redalen KR, Minn H, Malinen E, Ytre-Hauge KS. *Accounting for hypoxia in proton therapy planning with a FLUKA Monte Carlo based tool.* (Manuscript in preparation).

Conference contributions

Parts of the results included in this PhD thesis have been presented at several international medical physics conferences:

- **Dahle TJ**, Rykkelid AM, Stokkevåg CH, Görgen A, Edin NJ, Rørvik E, Fjæra LF, Malinen E, Ytre-Hauge KS. *Monte Carlo simulation of a low energy proton beam: Estimation of proton beam parameters and linear energy transfer distributions*. Nordic Association for Clinical Physics (NACP) symposium, February 2017, Oslo, Norway (oral presentation)

- **Dahle TJ**, Rykkelid AM, Stokkevåg CH, Görgen A, Edin NJ, Malinen E, Ytre-Hauge KS. *Monte Carlo simulations of a low energy proton beam and estimation of LET distributions*. European Society for Radiotherapy & Oncology (ESTRO) 36, May 2017, Vienna, Austria (oral presentation)

- **Dahle TJ**, Magro G, Stokkevåg CH, Ytre-Hauge KS, Mairani A. *Sensitivity of the Microdosimetric Kinetic Model to variations in model parameters*. Biology-Guided Adaptive Radiotherapy (BiGART) June 2017, Aarhus, Denmark (poster)

- **Dahle TJ**, Magro G, Stokkevåg CH, Ytre-Hauge KS, Mairani A. *Sensitivity study of the Microdosimetric Kinetic Model input parameters for carbon ion radiotherapy*. ESTRO 37, April 2018, Barcelona, Spain (poster)

- **Dahle TJ**, Rusten E, Stokkevåg CH, Mairani A, Wright P, Forsback S, Silvoniemi A, Minn H, Malinen E, Ytre-Hauge KS. *A FLUKA Monte Carlo code tool for RBE-modelling in proton therapy of hypoxic head and neck cancer*. Particle Therapy Co-Operative Group (PTCOG) 58, June 2019, Manchester, England (oral presentation)

Publication contributions

Other publications from the PhD period, but not part of the thesis:

- Rørvik E, Thörnqvist S, Stokkevåg CH, **Dahle TJ**, Fjæra LF, Ytre-Hauge KS (2017). *A phenomenological biological dose model for proton therapy based on linear energy transfer spectra.* Medical physics, 44(6), 2586-2594.

- Rørvik E, Fjæra LF, **Dahle TJ**, Dale JE, Engeseth GM, Stokkevåg CH, Thörnqvist S, Ytre-Hauge, KS (2018). *Exploration and application of phenomenological RBE models for proton therapy.* Physics in Medicine & Biology, 63, 185013.

- Ytre-Hauge KS, Fjæra LF, Rørvik E, **Dahle TJ**, Dale JE, Thörnqvist S and Stokkevåg CH. *Inter-patient variations in relative biological effectiveness for cranio-spinal irradiation with protons.* (Submitted to Scientific Reports).

List of abbreviations

[^{18}F]-EF5	2-(2-nitro-^{1}H-imidazol-1-yl)-N-(2,2,3,3,3-pentafluoropropyl)-acetamide labeled with ^{18}F
[^{18}F]-FMISO	^{18}F-fluoromisonidazole
CHO	Chinese hamster ovary cells.
CNAO	National Center for Oncological Hadrontherapy, Italy
CSDA	Continuous slowing down approximation
CT	Computed tomography
CTV	Clinical target volume
DICOM	Digital Imaging and Communications in Medicine
DVH	Dose volume histogram
FWHM	Full width at half maximum
GTV	Gross tumor volume
HIT	Heidelberg Ion-beam Therapy Center, Germany
HNC	Head and neck cancer
HSG	Human salivary gland tumor cells
ICRU	International Commission on Radiation Units and Measurements
KC model	Kiefer-Chatterjee track structure model
LEM	Local effect model
LET	Linear energy transfer
LET_d	Dose-averaged LET
LQ model	Linear quadratic model
MC	Monte Carlo
MKM	Microdosimetric kinetic model
MRI	Magnetic resonance imaging
NIRS	National Institute of Radiological Sciences, Japan
OAR	Organ at risk
OCL	Oslo Cyclotron Laboratory
OER	Oxygen enhancement ratio

PET	Positron emission tomography
pO_2	Partial oxygen pressure
PTV	Planning target volume
RBE	Relative biological effectiveness
ROR	RBE model by Rørvik *et al* (2017)
SOBP	Spread-out Bragg peak
T1	T1 tumor cells
TCP	Tumor control probability
T/M ratio	Tumor-to-muscle ratio
TPS	Treatment planning system
V79	Chinese hamster V79 cells

Contents

Scientific environment iii

Acknowledgements v

Abstract vi

List of publications viii

Conference contributions ix

List of abbreviations xi

Contents xiii

1. Introduction 1

2. Physics of Particle Therapy 3

2.1 Interaction of particles with matter 3

2.2 Physical dose and depth dose curves 6

2.3 Linear energy transfer 7

2.4 Microdosimetry 8

3. Radiobiology 11

3.1 Linear quadratic model 11

3.2 Relative biological effectiveness 12

3.3 Tumor hypoxia 15

4. Treatment Planning 17

4.1 Treatment planning systems 17

4.2 Recalculation of treatment plans in FLUKA 18

4.3 Clinically applied RBE models in carbon ion therapy 19

5. Thesis Objective 23

6. Materials and Methods 25

6.1 Implementation of a cell irradiation setup in FLUKA 25

6.2 Study of the microdosimetric kinetic model 26

6.3 A biological dose method accounting for hypoxia 30

6.4 Ethical considerations 33

7. Summary of Results 35

7.1 More accurate knowledge of the LET for cell experiments 35

7.2 Study of a clinical RBE model 36

7.3 Including hypoxia in biological dose calculations 38

8. Discussion 41

8.1 Improving RBE measurement data 42

8.2 Applying variable RBE models clinically 45

8.3 Including hypoxia in biological dose calculations 48

9. Conclusions 51

References 53

Publications 61

1. Introduction

Cancer is a group of diseases caused by uncontrolled division of abnormal cells in parts of the body. While diagnostics and treatment modalities for cancer have improved greatly the last century with substantially increased survival rates (Quaresma *et al* 2015), cancer is still the second leading cause of death worldwide (WHO 2018). Methods for treating cancer are therefore still in continuous development, and these include radiotherapy, which has a vital role in cancer treatment. The aim of radiotherapy is to kill the cancer cells while sparing the healthy tissue. In conventional radiotherapy, the patients are treated with photons or electrons. However, due to the physical properties of particles like protons and heavier ions, it can be advantageous to use these in radiotherapy (Durante *et al* 2017). Radiotherapy with protons and heavier ions is called particle therapy, and is currently under planning in Norway, with two proton therapy centers expected to open in Oslo and Bergen before 2025.

Radiotherapy dates back to the end of the 19th century, with three fundamental discoveries; the discovery of x-rays by Wilhelm Röntgen in 1895 (Röntgen 1896), followed by the discovery of natural radioactivity by Henri Becquerel in 1896 (Becquerel 1896) and the discovery of polonium and radium by Marie and Pierre Curie in 1898 (Curie 1950). The use of x-rays in cancer treatment was suggested shortly after Röntgen's discovery, and already in 1896 x-rays were applied in patient treatment (Lederman 1981). In 1904, Wilhelm Henry Bragg studied α-particles emitted by radium, and discovered that the α-particles ionize most efficient towards the range of the particle (Bragg and Kleeman 1904). This ionization peak is now called the Bragg peak, and Robert R. Wilson suggested in 1946 that this effect could be used in cancer treatment applying protons and heavier ions (Wilson 1946).

Particle therapy has evolved drastically since being suggested by Wilson, from being only offered in research facilities to state-of-the-art treatment facilities at hospitals. Initially, several particle types, including helium, carbon, neon and

argon ions, were used in patient treatment (Castro *et al* 1980). Today, only protons and carbon ions are applied clinically, however, helium ions are about to make a comeback, with Heidelberg preparing to start treatments with helium in 2020 (RaySearch 2019). There are currently more than eighty proton therapy facilities worldwide, found in Europe, Asia, North America and South Africa, while carbon ion therapy is currently offered in thirteen facilities, in Japan, Europe and China (PTCOG 2019).

Protons and heavier ions have, as mentioned, physical properties which makes it possible to better confine the dose to the target when compared to conventional radiotherapy. Another difference is that protons and heavier ions also have an increased relative biological effectiveness (RBE) compared to photons. In particle therapy, an RBE-weighted dose (biological dose) is therefore applied in treatment planning. A large amount of data has demonstrated that the RBE varies with parameters such as physical dose, biological endpoint, the linear energy transfer (LET) and tissue type (Paganetti 2014). Still, a constant RBE of 1.1 is currently applied at clinical proton centers, as recommended by ICRU (ICRU 2007), ignoring these RBE dependencies. For heavier ions the variations in RBE are too large to be ignored. Therefore, clinical carbon therapy facilities generally apply variable RBE models, with the local effect model (LEM) in Europe (Scholz and Elsässer 2007) and the modified microdosimetric kinetic model (MKM) in Japan (Inaniwa *et al* 2015).

Monte Carlo codes are useful tools in dose calculations, and regarding the dosimetric accuracy, general purpose Monte Carlo codes are considered the gold standard (Kozłowska *et al* 2019). In this thesis, the FLUKA Monte Carlo code (Böhlen *et al* 2014, Ferrari *et al* 2005) has been used to study the biological dose in particle therapy, first as a tool to improve *in vitro* data for RBE calculations, second for comparing and studying a clinically applied biological dose model and last to develop and study a new biological dose calculation method which accounts for both the traditional RBE dependencies and the tumor oxygen levels in a patient.

2. Physics of Particle Therapy

Radiotherapy utilizes ionizing radiation in treatment of cancer, which is radiation with enough energy to detach electrons from atoms or molecules. The goal of radiotherapy is to damage the cancer cell DNA enough to kill the cells, while at the same time sparing the surrounding healthy cells. The DNA is damaged either by direct action, which happens when the radiation has enough energy to directly break parts of the DNA, or indirect action, which is when the radiation creates free radicals which may be harmful for the DNA (Joiner and van der Kogel 2009). The energy deposited in matter by the radiation per unit mass is called the radiation dose, and the aim is to deposit enough dose in the tumor to kill it.

2.1 Interaction of particles with matter

In particle therapy, the protons or heavier ions interact with the matter mainly through inelastic Coulomb scattering, elastic Coulomb scattering and non-elastic nuclear reactions, illustrated in Figure 2.1. Through these interactions the particles will lose energy, be deflected or removed from the original particle trajectory, ionize atoms and create secondary particles.

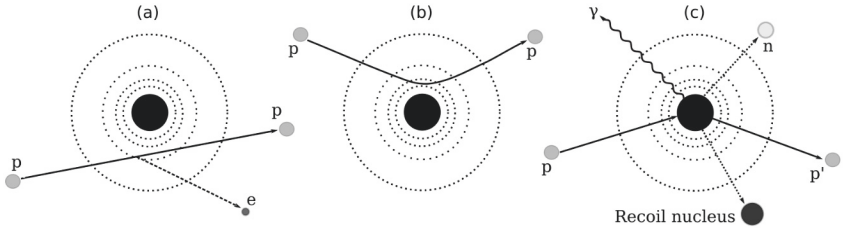

Figure 2.1: Interaction of protons with matter: inelastic Coulomb scattering (a), elastic Coulomb scattering (b) and non-elastic nuclear reaction (c). Abbreviations: p: primary proton, p': secondary proton, e: electron, n: neutron, γ: gamma rays. The figure is adapted from Newhauser & Zhang (2015).

2.1.1 Stopping power

In inelastic Coulomb scattering, the incoming particle interacts with an atomic electron. The electron will be freed from the atom, while the primary proton or carbon ion, which is significantly heavier than the electron, will continue in an

approximately straight line, however, with a slightly lower energy (Newhauser and Zhang 2015). The energy loss rate is generally called the stopping power of the particles, and is described by the Bethe-Bloch equation, here as given in Leo (2012):

$$-\frac{\mathrm{d}E}{\mathrm{d}x} = 2\pi N_a r_e^2 m_e c^2 \rho \frac{Z}{A}\frac{z^2}{\beta^2}\left[\ln\left(\frac{2m_e\gamma^2 v^2 W_{\max}}{I^2}\right) - 2\beta^2 - \delta - 2\frac{C}{Z}\right]. \quad (2.1)$$

Here, E is the mean energy loss over distance x, N_a is Avogadro's number, r_e is the classical electron radius, m_e is the electron mass, c is the speed of light in vacuum, ρ is the density of the absorbing material, Z and A are the atomic number and atomic weight of the absorbing material, respectively, z is the projectile charge, β is the projectile velocity relative to the speed of light, $\gamma = (1-\beta^2)^{-1/2}$, v is the projectile velocity, $W_{\max}$ is the maximum energy transfer in a single collision, I is the mean excitation potential and δ and C are correction terms.

The particle stopping power is proportional to the square of the charge and inversely proportional to the square of the velocity of the primary proton or carbon ion (Equation (2.1)). The stopping power will therefore increase with decreasing velocity, and the energy loss is therefore highest when the particle has almost stopped, leading to the characteristic Bragg peak in the depth dose distribution. As carbon ions are heavier than protons, carbon ion therapy requires a higher energy to produce the same stopping power as protons, as seen in Figure 2.2.

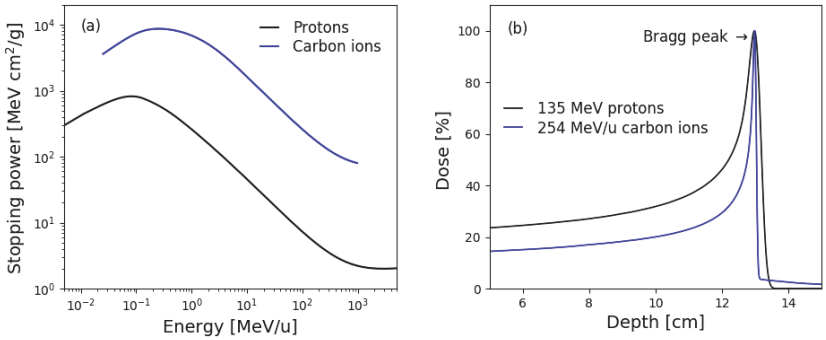

Figure 2.2: Stopping power in water as a function of energy for protons and carbon ions (a), together with depth dose profiles of a 135 MeV proton and a 254 MeV/u carbon ion beam in water (b). Stopping power data from ICRU49+73, obtained using the generic stopping power library libdEdx (Lühr *et al* 2012). The depth dose distributions were obtained through FLUKA Monte Carlo simulations.

2.1.2 Range

The particle range is defined as the depth at which half of the primary particles have come to rest (Newhauser and Zhang 2015). This is an average quantity, due to variations in the energy loss of the individual particles called range straggling. The range of particles can be calculated according to the continuous slowing down approximation (CSDA), i.e. by integrating the particle stopping power from zero to the initial particle energy (Fano 1953). Several stopping power and range tables have also been made, which makes easy to directly get the range of particles in a given medium (Lühr *et al* 2012).

Range straggling broadens the Bragg peak of the beam. The ratio of the straggling width and the mean range is proportional to $1/\sqrt{M}$, where M is the particle mass (Schardt *et al* 2010). Carbon ions will therefore have a much smaller straggling width compared to protons when they have the same range. This explains the much sharper Bragg peak of carbon ions compared to protons, seen in Figure 2.2b. When irradiating a patient, however, the profile of the Bragg peaks will be even broader, due to for instance the density homogeneities of the penetrated tissue (Schardt *et al* 2010).

2.1.3 Lateral dose profile

The width of a particle beam traveling through a medium will be broadened due to particles passing close enough to nuclei to be elastically scattered or deflected by the positive charge of the nuclei (Newhauser and Zhang 2015). While the angular deflection of a single scattering can be negligible, the sum of the scattering can result in a large deflection from the original path. This effect is therefore called multiple Coulomb scattering, and results in an observable lateral broadening of the beam with a nearly Gaussian distribution. The lateral broadening is more than three times larger for a proton beam than for a carbon ion beam at the same range, which is a clinical disadvantage for protons (Weber and Kraft 2009). This broadening may be slightly reduced by reducing the air gap between patient and beam exit window (Weber and Kraft 2009). By comparison, photons will often have a lateral broadening between protons and carbon ions (Rath and Sahoo 2016).

2.1.4 Production of secondaries

In non-elastic nuclear reactions, the primary particle will interact with an atomic nucleus, leading to a reduction in the primary particle fluence and the production of secondary particles. For this to happen, the primary particles must have enough energy to overcome the Coulomb barrier of the nucleus (Newhauser and Zhang 2015). In proton therapy, the most common secondary particles are secondary protons and neutrons. Secondary protons may deposit as much as 10% of the absorbed dose in a high-energy proton treatment beam, while neutrons are extremely penetrating and have an RBE of as much as 20 times higher than the proton RBE, potentially leading to an increased risk of radiogenic late effects (Newhauser and Zhang 2015). In carbon ion therapy, secondary ions with lower atomic number than carbon may be produced, as well as neutrons and target fragments. The secondary ions with lower atomic number than carbon ions have longer range than the primary particles (at the same velocity), leading to a fragmentation tail after the Bragg peak (Gunzert-Marx *et al* 2008). This fragmentation tail leads to a dose deposition after the Bragg peak of the carbon ions, as observed in Figure 2.2b.

2.2 Physical dose and depth dose curves

2.2.1 Absorbed dose

The absorbed dose (physical dose) is a physical quantity describing the mean energy imparted by ionizing radiation to matter (ICRU 2011). The unit of absorbed dose is gray (Gy), where 1 Gy = 1 J/kg. In conventional radiotherapy, the absorbed dose is the standard when reporting the delivered dose to a patient, while in particle therapy this dose will be modified to account for biological effects also, as described further in Chapter 3.

2.2.2 Spread-out Bragg peak

In a clinical scenario, the particle beam must cover an extended area, which is not possible with a monoenergetic beam. This leads to the spread-out Bragg peak (SOBP), where particle beams with different energies form a uniform dose to the

target area (Figure 2.3). This energy modulation is achieved by either introducing appropriate filters in the beamline or by tuning the accelerator to deliver beams with different energies. While this will give radiation dose outside the tumor area, it is still favorable compared to the depth dose curve of conventional radiotherapy with photons.

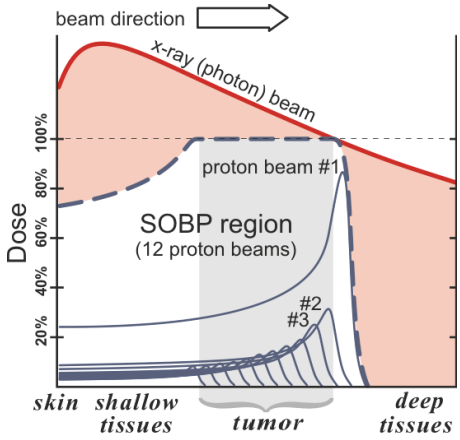

Figure 2.3: Comparison of photon and proton depth dose distributions. The figure is adapted from Filipak (2012).

2.3 Linear energy transfer

Linear energy transfer (LET) is a measure of a charged particle's ionization density, and is defined as follows:

$$\mathrm{LET}_\Delta = \frac{\mathrm{d}E_\Delta}{\mathrm{d}l}, \tag{2.2}$$

where $\mathrm{d}E_\Delta$ is the mean energy lost by the charged particles due to electronic interactions when traversing the distance $\mathrm{d}l$, when excluding the transfer to electrons with energies above a maximum transfer energy Δ (ICRU 2011). LET_Δ is generally called the restricted LET, and it excludes secondary electrons (delta rays) with energies above Δ, as these electrons could deposit their energy relatively far from the origin. If all transferred energy is included in the calculation of the LET, the quantity is called the unrestricted LET (LET_∞) and equals the electronic stopping power of the particle. In the clinical energy range for protons and carbon ions, it can be assumed that there is little difference between LET_Δ and LET_∞ (Grzanka

2014). The unrestricted LET can, in infinitely small volumes, be related to the absorbed dose D as follows:

$$D = \frac{\Phi}{\rho}\mathrm{LET}, \tag{2.3}$$

where Φ is the particle fluence and ρ is the tissue density (Gottschalk 2016). This shows that fewer high-LET particles are needed to give the same absorbed dose as low-LET particles.

At a given position along the beam, there may be several particles with different energies, resulting in several LET values, i.e. an LET spectrum. However, a single LET value is often easier to work with, and the LET is therefore commonly averaged into for instance dose-averaged LET ($\mathrm{LET_d}$). From Equation (2.3), the $\mathrm{LET_d}$ at a position z can be found as follows:

$$\mathrm{LET_d}(z) = \frac{\int_0^\infty D(E,z)\cdot\mathrm{LET}(E)\mathrm{d}E}{\int_0^\infty D(E,z)\mathrm{d}E} = \frac{\int_0^\infty \Phi(E,z)\mathrm{LET}^2(E)\mathrm{d}E}{\int_0^\infty \Phi(E,z)\mathrm{LET}(E)\mathrm{d}E}, \tag{2.4}$$

where *D* is the absorbed dose contributed by charged particles with kinetic energy E at location z and Φ is the particle fluence. A clinical proton beam will typically have $\mathrm{LET_d}$ values less than 10 keV/µm, while clinical carbon ion beam can have $\mathrm{LET_d}$ values up to 200-300 keV/µm (Kantemiris *et al* 2011).

2.4 Microdosimetry

While the absorbed dose and LET are often applied when determining the damage done by the radiation, they may not always be sufficient to describe the effectiveness of the radiation (Liamsuwan *et al* 2014). For better describing this, more complete information of energy depositions at the subcellular level can be required. Microscopic quantities like the lineal energy and specific energy may therefore be useful here. The LET and absorbed dose differ from microdosimetric quantities as they quantify the average energy loss of charged particles per distance or volume, while the stochastic energy deposition in micrometric volumes is measured in microdosimetry (ICRU 1983).

2.4.1 Specific energy and lineal energy

The specific energy (z) and lineal energy (y) are microdosimetric quantities corresponding to the absorbed dose and the LET. The specific energy is defined as the quotient of the energy, ε, imparted by ionizing radiation in a volume of mass m, while the lineal energy is the quotient of the energy, ε_s, imparted to the matter in a given volume with a mean chord length of $\bar{l}$ by a single energy-deposition event:

$$z = \frac{\varepsilon}{m}, \tag{2.5}$$

$$y = \frac{\varepsilon_s}{\bar{l}}. \tag{2.6}$$

The specific energy has unit Gy, while the lineal energy has unit keV/µm. The lineal energy can be measured directly, and the specific energy can be directly calculated from this. While the gold standard of microdosimetric measurements is tissue equivalent proportional counters, silicon-on-insulator microdosimeters have been developed as an alternative, which increases the spatial resolution significantly (Rosenfeld 2016). However, it can be more practical to estimate the specific energy using track structure models, which can give the specific energy to a volume as a function of the distance from the ion trajectory to the center of the volume (Inaniwa *et al* 2010).

2.4.2 Track structure models

When protons or heavier ions ionize atoms, the secondary electrons will generally move a distance of a few nanometers to a few millimeters from the particle trajectory and deposit dose. To describe the radial dose distribution from ion trajectories, track structure models may be used. In carbon ion therapy, the Kiefer-Chatterjee track structure model (Chatterjee and Schaefer 1976, Kiefer and Straaten 1986) and a track structure model by Scholz & Kraft (1996) is applied in biological dose calculations in Japan and Europe, respectively. These models estimate similar dose distributions from individual tracks, except close to the center of the track, as observed in Figure 2.4.

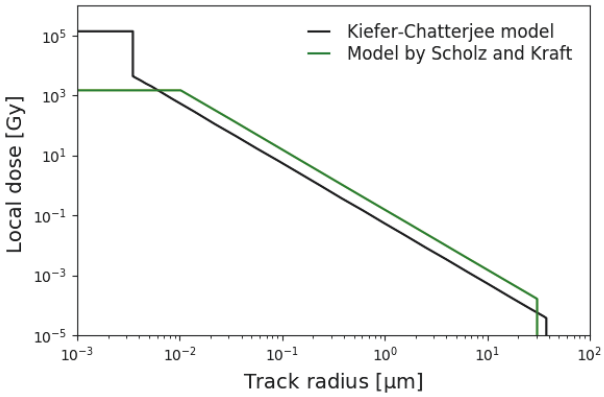

Figure 2.4: Track structure for 43 MeV/u carbon ions with LET = 50 keV/µm calculated by the Kiefer-Chatterjee model and the model by Scholz and Kraft. The figure is reproduced from Kase *et al* (2008) with permission from IOP Publishing.

3. Radiobiology

When irradiating a biological system, a succession of processes will happen. A time after the physical processes have taken place, the biological phase will start. This will happen from seconds to years after irradiation, depending on the type and severity of the damages (Joiner and van der Kogel 2009). In the biological phase, measurable changes to the organism can be seen. While the majority of lesions from the radiation are successfully repaired in this phase, some will fail to do this and this may eventually lead to mutation or cell death (Joiner and van der Kogel 2009). The biological effects resulting from irradiation with protons and heavier ions will be enhanced compared to irradiation with photons. In the following, the linear quadratic (LQ) model, which quantifies the radiosensitivity of cells, and the RBE will be described. This will be followed by a description of tumor hypoxia, which is a situation where the tumor has areas with low oxygen levels, resulting in lower cell radiosensitivity.

3.1 Linear quadratic model

The most common way of describing cell survival after irradiation is by the LQ model. In this model, the cell survival fraction *S* is given by

$$-\ln(S) = \alpha D + \beta D^2, \tag{3.1}$$

where D is the physical dose and α and β are radiosensitivity parameters. The α and β parameters are generally found by fit to experimental data, and the α/β-ratio is commonly used to describe the fractionation sensitivity of the cells.

Studies of tissue responses to radiation have shown that tumors and early responding tissues (e.g. skin, oral mucosa and bone marrow) generally have $(\alpha/\beta)_x$-ratios (i.e. the α/β-ratio of photons) in the order of 7-10 Gy, while late responding tissues (e.g. heart, lung and kidney) generally have $(\alpha/\beta)_x$-ratios in the order of 3-5 Gy (McMahon 2019). The higher the α/β-ratio of the cell line, the lower the fractionation sensitivity (Leeuwen *et al* 2018).

3.2 Relative biological effectiveness

The RBE is defined as the ratio of the physical doses of a reference radiation, $D_{\text{reference}}$, (generally photon radiation) and of the radiation in question, D_p, which results in the same biological effect for a given endpoint (IAEA 2008):

$$\text{RBE} = \frac{D_{\text{reference}}}{D_p}. \tag{3.2}$$

The biological endpoint can vary; however, for *in vitro* studies it is often set to 10% cell survival, as illustrated in Figure 3.1. From the LQ model (Equation (3.1)) and the definition of the RBE, the RBE can be calculated as follows:

$$\text{RBE} = \frac{1}{D_p}\left(\sqrt{\left(\frac{\alpha_x}{2\beta_x}\right)^2 + \frac{(\alpha D_p + \beta D_p^2)}{\beta_x}} - \frac{\alpha_x}{2\beta_x}\right), \tag{3.3}$$

where D_p is the physical dose of the particles (e.g. proton or carbon ion) and α, β, α_x and β_x are the particle and photon radiosensitivity parameters, respectively.

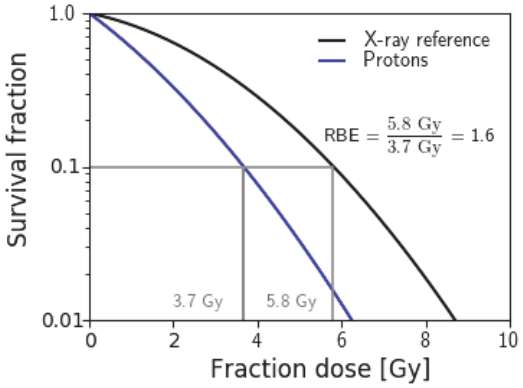

Figure 3.1: Survival fraction curves of V79 cells irradiated with x-rays and 20 keV/µm protons, and corresponding RBE calculation at 10% cell survival. Based on data from Belli *et al* (1998).

3.2.1 Biological dose

The prescribed dose in particle therapy is based on the biological dose (also called RBE-weighted dose), which is illustrated in Figure 3.2. The biological dose, D_{bio} is calculated as follows:

$$D_{bio} = \text{RBE} \cdot D_{phys}, \tag{3.4}$$

where D_{phys} is the total physical dose. Clinically, the RBE in proton therapy is set constant and equal to 1.1, ignoring variations in the RBE, while in carbon ion therapy the RBE is determined by variable RBE models.

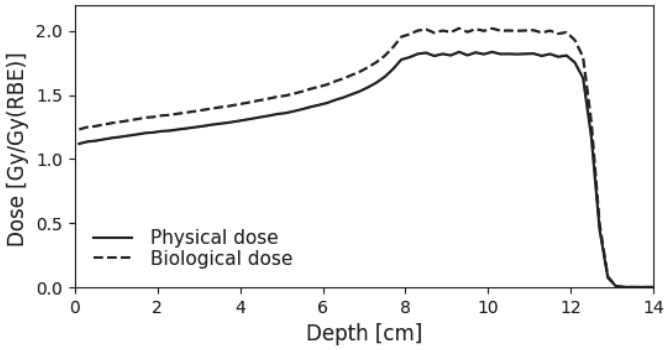

Figure 3.2: Physical dose of a proton spread-out Bragg peak (solid line), with corresponding biological dose (dashed line). Here, the RBE was set to 1.1. To distinguish from physical dose, the biological dose has the unit Gy(RBE). The depth dose distributions were obtained through FLUKA Monte Carlo simulations.

3.2.2 RBE models

In order to estimate the variable RBE in particle therapy, several RBE models have been developed. These models can generally be divided into two categories. The first category is phenomenological models, which considers the particle interactions within the cell and the subcellular effects to be a "black box" and therefore attempts to estimate biological effects directly by fitting to experimental data. The second category is mechanistic/biophysical models, which attempts to model the underlaying biological effects on a micrometer scale within the cells. Most phenomenological and biophysical RBE models are based on the general RBE equation (Equation (3.3)). The difference between the models will be in the definition of the radiosensitivity parameters α and β of the particles, as well as in the values used for the photon radiosensitivity parameters α_x and β_x. An extensive review of the existing phenomenological RBE models for proton therapy can be found in Rørvik *et al* (2018). In carbon ion therapy, more sophisticated phenomenological models or biophysical models are required, due to the "overkill effect" at high LET values (Karger and Peschke 2018). Currently in clinical carbon

ion therapy, biophysical models are applied in treatment planning, and these are described further in Section 4.3. However, a phenomenological model has been applied earlier in Japan (Karger and Peschke 2018, Kanai *et al* 1999).

3.2.3 RBE dependencies

Cell experiments have shown that the RBE is dependent on several factors, including the biological endpoint, particle type, tissue type, radiation quality and the physical dose (Paganetti 2014). In RBE models, the dependency on the biological endpoint is generally covered by the experimental data the model is fitted to, while the physical dose dependency is covered by the dose input in the RBE model (Equation (3.3)). The dependencies on radiation quality, particle type and tissue type are covered in the definition of the radiosensitivity parameters, and this is where RBE models mainly differ.

The radiation quality is often quantified by the LET. The RBE will generally increase with increasing LET, except at high LET values due to the so-called overkill effect, as illustrated in Figure 3.3. This increase in RBE with increasing LET can be explained by high-LET radiation having denser track structure than low-LET radiation, leading to more severe damage where the track intersects vital structures such as the DNA (Joiner and van der Kogel 2009). It is widely accepted that the LET amplifies at the distal end of the particle beam, and the RBE will therefore generally increase with depth of the beam. The radiation quality can also be quantified by the specific energy or lineal energy, and studies have shown that these quantities may be more accurate than LET when quantifying the radiation quality (Kase *et al* 2006, Liamsuwan *et al* 2014).

The RBE versus LET data in Figure 3.3a show that the RBE is also dependent on the particle type. The maximum LET values for protons are much lower than the ones for carbon ions, and protons will therefore generally have lower RBE values, although protons will generally be more effective than carbon ions for the same LET values (Durante and Paganetti 2016). From the data in Figure 3.3b, a dependency on cell lines can also be observed. While the general trend between the data of these cell lines are similar, the magnitude of the RBE differs. The

survival fraction of cells is, as already mentioned, dependent on the tissue type, and studies have shown that this is reflected in the RBE, generally with an increasing RBE with decreasing cell line $(\alpha/\beta)_x$-ratio (Schardt *et al* 2010).

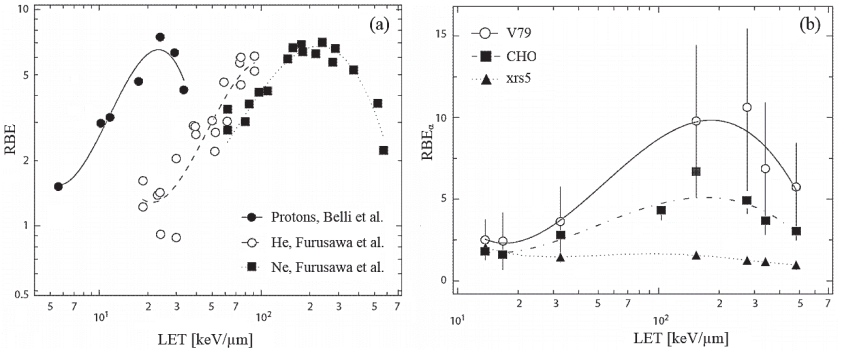

Figure 3.3: RBE as function of LET for different particle types (a) and for different cell lines irradiated with carbon ions (b). The figure is adapted from Scholz (2003) with permission from Springer.

3.3 Tumor hypoxia

Hypoxic cells are cells with low oxygen levels, and these are more radioresistant than normal cells (Fleming *et al* 2015). This effect is often quantified by the oxygen enhancement ratio (OER), which is the ratio of the dose at a given oxygen pressure (D_h) to that at a standard oxygen pressure (D_a), producing the same biological effect:

$$\mathrm{OER} = \frac{D_h}{D_a}, \tag{3.5}$$

as illustrated in Figure 3.4a. The OER decreases with increasing LET, and carbon ions can therefore be quite efficient against hypoxic cells, compared to protons and photons (Figure 3.4b). Hypoxia will therefore in general increase the RBE for carbon ions, while protons generally do not have high enough LET to make any significant difference in OER compared to photons, except towards the range of the proton beam (Wenzl and Wilkens 2011).

Tumor hypoxia arises when the supply of oxygen from the vasculature is less than the oxygen consumption in the tumor tissue (Koch and Evans 2015), and the level of hypoxia is frequently quantified by the partial oxygen pressure (pO_2). The

pO_2 values at hypoxic conditions are generally below 8-10 mmHg (Silvoniemi 2018), while the normal pO_2 in tissues may vary from this and up to almost 160 mmHg. While there is currently no perfect method for estimating tumor hypoxia, positron emission tomography (PET) imaging is normally the preferred method for detecting hypoxia in clinical scenarios (Fleming *et al* 2015).

Several methods for overcoming the issue with hypoxia in radiotherapy have been proposed. One method is to increase the oxygen levels in the tumor before treatment, and with this removing the problem before irradiation. An important goal here has been to modify the level of hemoglobin before the start of radiotherapy, however, this has not been observed to correct tumor hypoxia (Welsh *et al* 2017, Silvoniemi 2018). Other approaches, including breathing of carbogen (mixture of 98% oxygen and 5% carbon dioxide) to increase the tumor blood flow, have shown some potential, however, not enough to defend the inclusion of these methods in clinical practice (Silvoniemi 2018). Another method is to modify the treatment plan to take the oxygen levels into account. This includes dose painting, where increased radiation dose is prescribed to hypoxic subvolumes of the tumor (Malinen and Søvik 2015), and LET painting, where instead the LET is increased in the hypoxic areas in the tumor (Bassler *et al* 2014). Methods for including the OER in biological dose calculations have also been proposed (Tinganelli *et al* 2015, Scifoni *et al* 2013, Bopp *et al* 2016, Strigari *et al* 2018).

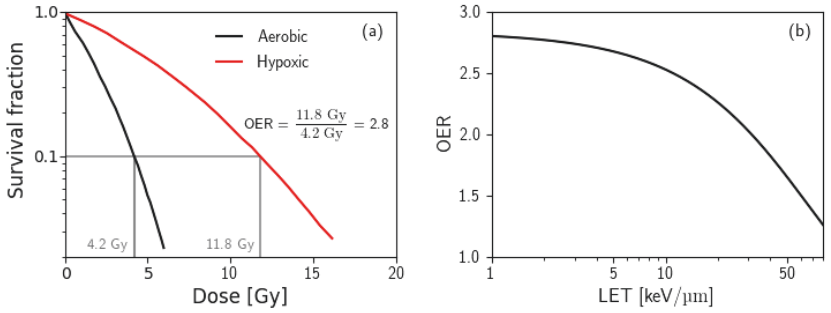

Figure 3.4: Survival fractions of aerobic and hypoxic cells irradiated with protons with dose-averaged LET of 17 keV/µm (a), and OER as a function of LET calculated at 10% cell survival with pO_2 of 160 mmHg and 0.01 mmHg for aerobic and hypoxic conditions, respectively (b). Figure to the left is based on data from Prise *et al* (1990), while figure to the right is created using OER model by Wenzl and Wilkens (2011a).

4. Treatment Planning

In radiotherapy, the goal is to irradiate the tumor with the prescribed dose while sparing the surrounding healthy tissue as well as possible. This requires careful treatment planning. To plan a treatment, computed tomography (CT) images of the patient are acquired, and several volumes are delineated: the gross tumor volume (GTV) describing the primary tumor; the clinical target volume (CTV) describing the extent of microscopic tumor spread around the GTV; the planning target volume (PTV) which adds margins around the CTV to allow for planning or delivery uncertainties; and relevant organs at risk (OAR) (Burnet *et al* 2004). A treatment planning system (TPS) is subsequently used to create the treatment plan. Dose volume histograms (DVHs) coupled with 2D dose distributions are used to get an overview of the dose in different regions of interest and to evaluate and compare the treatment plan to the prescribed target dose and dose constraints for the OAR.

4.1 Treatment planning systems

4.1.1 Analytical treatment planning systems

Clinically, fast treatment planning is a requirement, leading to a compromise between accuracy and computation time. Clinical dose distributions are therefore commonly planned and optimized in fast analytical dose calculation algorithms, which generally rely on pencil beam algorithms to calculate the dose (Schuemann *et al* 2015). Advanced treatment planning techniques use inverse treatment planning, where a dose is prescribed to the PTV, dose constraints are set to the OARs, and the TPS will use this to optimize the treatment plan to the best possible biological dose distribution.

The TPS will use patient information given in a DICOM (Digital Imaging and Communications in Medicine) format. The files required to perform treatment planning are DICOM CT images, which have anatomical information of the patient, and DICOM RT Struct, containing information on the delineated structures. After creating a treatment plan, information on this plan will be stored in the DICOM RT

Plan file, including (but not limited to) information on the treatment beams, dose prescription, patient setup, gantry angles, isocenter position and information on range shifters. Information on the dose distribution calculated by the TPS can be found in the DICOM RT Dose files and can be used to plot the dose distribution and DVHs.

4.1.2 Monte Carlo based treatment planning tool

While fast analytical TPSs are required for day-to-day clinical treatment planning, they have some limitations, especially in difficult and non-standard treatment scenarios, involving for instance tissue heterogeneities or metallic implants (Mairani *et al* 2013). Monte Carlo codes will give more accurate dose calculations, and are therefore considered the "gold standard" for dosimetric calculations (Kozłowska *et al* 2019). A second issue with commercial TPSs is that they generally do not include any RBE models for protons or only include one RBE model for carbon ions, making research impractical. Mairani *et al* (2013) therefore created a Monte Carlo based treatment planning tool, using the FLUKA Monte Carlo code (Böhlen *et al* 2014, Ferrari *et al* 2005). This tool re-optimizes an initial treatment plan, created for instance in a clinical TPS. The re-optimization can be performed with any RBE model which follows the general RBE formula given in Equation (3.3) in Section 3.2 and which is implemented FLUKA. While this tool works well for research, it uses much more computational time than the commercial TPSs and is therefore not ideal for clinical use.

4.2 Recalculation of treatment plans in FLUKA

Our group at the University of Bergen has an in-house made system based on the FLUKA Monte Carlo code for recalculation of intensity modulated proton therapy treatment plans applying different RBE models (Fjæra *et al* 2017). This tool can automatically translate the information on the treatment plan from DICOM files to files readable by FLUKA. This includes information on the radiation beam (beam energies, spot positions, spot sizes, spot weights and beam directions), which FLUKA reads through the *source* user routine, and scripts for translating the CT

image into FLUKA geometry and scoring regions. The RBE model used in the recalculation is defined in the *fluscw* (FLUence SCoring Weight) user routine. After the simulation, the quantities scored by FLUKA can be converted into a biological dose distribution in a DICOM RT Dose format. The tool also includes a script for plotting and comparing RT Dose files.

4.3 Clinically applied RBE models in carbon ion therapy

The main RBE models in clinical use are the local effect model (LEM) version I in Europe and the microdosimetric kinetic model (MKM) in Japan. The main model in Japan was previously a model developed by Kanai and co-workers (Kanai *et al* 1999), and this model is still applied at some centers (Fossati *et al* 2018). However, less was known about heavy-ion RBE when the Kanai model was developed and it is therefore based on several oversimplifications, ignoring for instance RBE dependencies on dose (Inaniwa *et al* 2015). Therefore, when the National Institute of Radiological Sciences (NIRS) in Japan changed their beam delivery system in 2011, the RBE model was changed from the Kanai model to the MKM (Inaniwa *et al* 2015). At the startup of carbon ion therapy at the Institute of Modern Physics (IMP) in China, a constant RBE of 2.5-3 was applied, however, the limitations of this strategy were fully acknowledged, also by the IMP (Fossati *et al* 2018). The MKM and LEM I give very different dose distributions, as seen in Figure 4.1. Therefore, to transfer clinical protocols between Europe and Japan, conversion factors must be applied, as done at Centro Nazionale di Adroterapia Oncologica (CNAO) in Italy (Molinelli *et al* 2016).

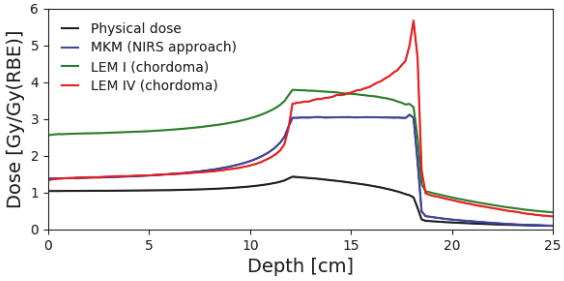

Figure 4.1: Biological dose in water as computed by the MKM (NIRS approach, blue), the LEM I (chordoma, green) and LEM IV (chordoma, red). The corresponding physical dose (black) is also shown. The depth dose distributions were obtained through FLUKA Monte Carlo simulations.

4.3.1 Microdosimetric kinetic model

The MKM predicts the cell survival response after ion irradiation from the specific energy deposited in a subcellular structure referred to as the 'domain'. The model also includes a saturation correction for expressing the decrease of RBE due to the overkill effect in high specific energy regions (Kase *et al* 2006). Therefore, when applying the MKM, the main parameter to estimate is the saturation-corrected dose-mean specific energy of the domain delivered in a single event ($z_{1\mathrm{D}}^{*}$) (Kase *et al* 2006).

The MKM applied in Japan is slightly modified from the general MKM. This model was introduced clinically at NIRS in Japan in 2011, simultaneously with the introduction of a new beam delivery method (Inaniwa *et al* 2015). At this point, the Japanese had almost 20 years of experience with carbon ion therapy, and they wanted to continue utilizing this experience. The reference radiation was therefore selected to be the center of a carbon ion SOBP with a width of 60 mm and energy of 350 MeV/u, assumed to be representative of clinical experience with carbon ion therapy at NIRS (Inaniwa *et al* 2015). Also, a scaling factor was introduced to the MKM, to make it possible to continue to use clinical protocols from the original system based on the Kanai model (Inaniwa *et al* 2015, Kanai *et al* 1999), as illustrated in Figure 4.2. In the Kanai model, the dose distribution is rescaled to utilize the clinical experience gained with fast neutron therapy at NIRS .

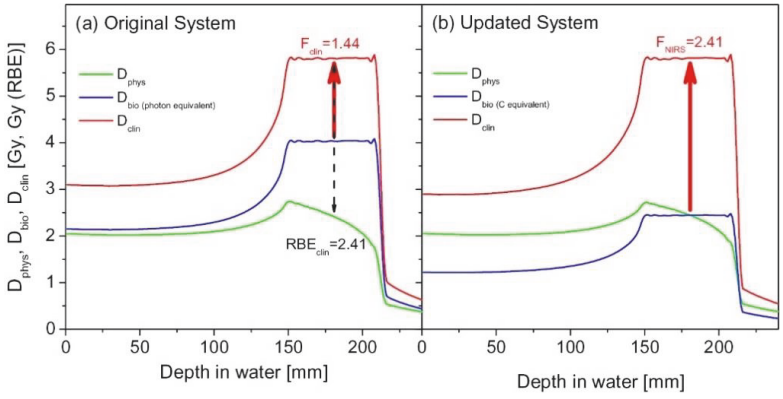

Figure 4.2: Dose planning of a 350 MeV/u carbon ion beam applying Japanese clinical dose systems: The original system applying the Kanai model (a) and updated system applying the MKM model (b). The figure is reprinted from Inaniwa *et al* (2015) with permission from IOP Publishing.

4.3.2 Local effect model

The LEM was developed and implemented for treatment planning within the carbon ion pilot project performed at GSI, Germany (Krämer and Scholz 2000), and is now applied in all European carbon ion therapy facilities. The LEM has been further developed since the first version, and the newest version is currently the LEM IV. However, only the first version has yet been applied clinically (Solov'yov 2017). The LEM I and IV varies significantly, as illustrated in Figure 4.1, and as the LEM I is the model applied clinically, further explanations of the LEM refers to the LEM I.

The LEM is based on the concept of 'local dose', defined as the expectation value of the energy deposition at any position in the radiation field for a given pattern of particle trajectories (Friedrich *et al* 2013a). The biological damage in a small subvolume of the cell nucleus is, in the LEM, solely determined by the local dose in that subvolume, independent of the particular radiation type leading to that local dose (Scholz and Elsässer 2007). While this is similar to the approach in the MKM, it is in the LEM applied to much smaller volumes (Scholz and Elsässer 2007). To calculate the local dose from the particles in the LEM, the radial dose distribution, estimated by a track structure model from Scholz & Kraft (1996), is needed together with the size of the critical target (Scholz *et al* 1997).

5. Thesis Objective

The overall goal of this project has been to contribute to the work of improving biological dose calculations in proton and carbon ion therapy. Increasing the accuracy of the biological dose calculations in clinical particle therapy may significantly improve treatments and working toward this goal is therefore important for the treatment outcome of patients. The work in this thesis involved performing Monte Carlo simulations to achieve more accurate *in vitro* RBE data, to study an existing clinical RBE model and to develop new methods for biological dose calculations in particle therapy. The specific objectives of each of the papers are described in the following.

Paper I:

- To implement and benchmark the low-energy proton beam cell irradiation experiment at the Oslo Cyclotron Laboratory in the FLUKA Monte Carlo code
- To estimate LET_d and LET spectra in the cell irradiation positions properly, using the FLUKA implementation

Paper II and III:

- To implement the biological dose model applied clinically in carbon ion therapy in Japan (the MKM) in FLUKA (Paper II)
- To use the FLUKA implementation to study the sensitivity of the MKM with respect to uncertainties in model parameters (Paper III)

Paper IV and V:

- To develop a method which includes patient oxygen levels acquired from [^{18}F]-EF5 PET images in proton biological dose calculations (Paper IV)
- To implement this biological dose calculation method in FLUKA (Paper IV) and in the FLUKA based treatment planning tool (Paper V)
- To study the effect of hypoxia on the proton biological dose distribution (Paper IV and V)

6. Materials and Methods

6.1 Implementation of a cell irradiation setup in FLUKA

The Oslo Cyclotron Laboratory (OCL) has an MC-35 cyclotron (Scanditronix, Lund, Sweden), which was used in a cell irradiation experiment. The setup of this experiment (illustrated in Figure 6.1) was implemented in the FLUKA Monte Carlo code (Paper I), in order to estimate the dose, LET spectra and LET_d in the cell irradiation positions. The setup geometry was first implemented in FLUKA, and then the initial beam parameters (beam energy, energy spread and lateral shape of the beam) were determined. The beam parameters were determined by comparing Monte Carlo simulated dose with dose measurements acquired using an Advanced Markus ionization chamber and Gafchromic (EBT3) dosimetry films at the three cell irradiation positions.

After implementation, the Monte Carlo simulations were used to estimate spatial variations in dose and LET in the cell irradiation positions. Water equivalent material was used in the cell positions in the simulations, instead of implementing the actual cell compositions. The resulting LET spectra were compared with LET spectra from a fictive 80 MeV proton beam (representing a clinical low-energy proton beam), at positions with equal LET_d values.

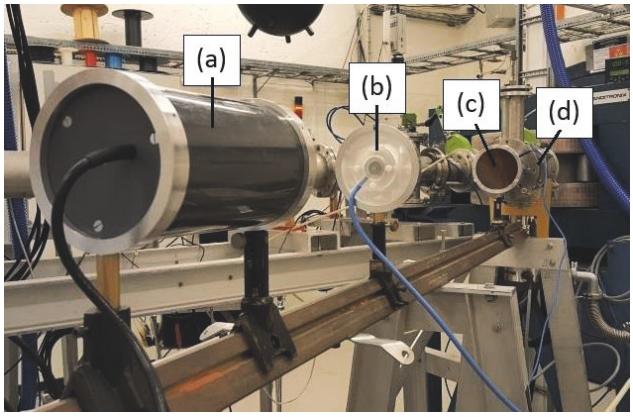

Figure 6.1: The cell irradiation setup at the Oslo Cyclotron Laboratory: the cell container (a), ionization chamber (b), monitor chamber (c) and beam exit window (tungsten) (d). During cell irradiation the ionization chamber is removed and replaced by the cell container.

6.1.1 LET calculations

The LET spectra were estimated at selected depths in the cell irradiation positions using the USRYIELD scoring card in FLUKA. This was done by dividing the cell irradiation positions into several regions and defining the scoring depths at the boundary crossings between two and two regions. The LET was estimated for protons (both primary and secondary) only.

The LET_d for protons was estimated in FLUKA using the *fluscw* user routine. This user routine multiplies the particle fluence (Φ) by a user defined quantity. The LET was estimated in *fluscw* using the internal FLUKA function GETLET(), and from this, the quantities $\mathrm{LET}^2 \times \Phi$ and $\mathrm{LET} \times \Phi$ were scored in each scoring voxel. As the LET_d for protons was estimated, Φ is the proton fluence. The LET_d in each voxel was then found by dividing these two scored values, following the method described in Section 2.3.

6.2 Study of the microdosimetric kinetic model

The biological dose model applied at NIRS in Japan (the MKM) was implemented in FLUKA (Paper II) by defining the radiosensitivity parameters α and β in the *fluscw* user routine. This makes it possible to score $\alpha \times \mathrm{LET} \times \Phi$, $\sqrt{\beta} \times \mathrm{LET} \times \Phi$ and $\mathrm{LET} \times \Phi$ in FLUKA, where Φ is the particle fluence and $\mathrm{LET} \times \Phi$ is the dose to water (see Equation (2.3) in Section 2.3). From this, the RBE was calculated as in Equation (3.3) in Section 3.2. In the MKM, β is a constant, while α is a function of the saturation-corrected dose-mean specific energy of the domain delivered in a single event (z_{1D}^*), which cannot be estimated directly in FLUKA. Tables connecting the particle energy to z_{1D}^* were therefore created, and a method for reading these tables was implemented in the *fluscw* user routine. To quantify the agreement between the FLUKA implementation and the NIRS TPS, comparisons were done between our specific energy calculations and biological dose estimates and corresponding calculations from Japan.

The sensitivity of the MKM to uncertainties in model parameters was then studied (Paper III). The MKM input parameters are the domain radius, r_d, the nucleus radius, R_d, and the radiosensitivity parameters α_x and β, and the values of

these parameters applied clinically are based on human salivary gland tumor (HSG) cells. The sensitivity study was done by varying the model parameters by $\pm\{5, 25, 50\}\%$, as well as comparing the HSG parameter set with parameter sets estimated using V79, CHO and T1 cells. Each time either r_d, R_d or β was changed, new specific energy tables had to be generated for FLUKA. The impact of the variations was studied on spread-out Bragg peak scenarios in water, and on a clivus chordoma patient.

6.2.1 Estimating the saturation-corrected dose-mean specific energy

When creating tables for estimating z_{1D}^*, the first step is to calculate the specific energy, z. This is the energy imparted to the domain divided by the mass of the domain, and was estimated based on the same method and assumptions as in Inaniwa *et al* (2010): the domain is assumed to be a cylindrical volume; the trajectories of the incident ions are parallel to the cylindrical axis of the domain; changes in ion trajectory and speed during the passage of the domain can be neglected; the ions constantly generate dose-track structures specific to the ion type and energy; and the whole target is composed of water. The specific energy to the domain from an ion was estimated using the Kiefer-Chatterjee (KC) track structure model (Section 2.4.2). The KC model gives the local dose as a function of track radius r, ion type (given by the effective charge of the ion, z_{eff}), particle energy E and LET. This dose will in the following be referred to as $D_{KC}(z_{eff}, r, E, \mathrm{LET})$, see Paper III for the entire function.

When an ion has an impact parameter x, i.e. a trajectory in the distance x from the center of the domain, there are three possible scenarios for a given distance ($r_i - \frac{1}{2}\Delta r$) from the track which describes the volume of the domain receiving dose, as illustrated in Figure 6.2. The specific energy to the domain for this impact parameter will then be the sum of the dose contributions to the domain from each given distance from the ion trajectory multiplied by the volume receiving this dose, divided by the total volume of the domain:

$$z\left(x, z_{eff}, E, \mathrm{LET}\right) = \frac{\sum_i D_{KC}\left(z_{eff}, r_i - \frac{1}{2}\Delta r, E, \mathrm{LET}\right) \cdot \Delta V(r_i, \Delta r, x)}{\pi r_d^2 R} = \frac{\sum_i D_{KC}\left(z_{eff}, r_i - \frac{1}{2}\Delta r, E, \mathrm{LET}\right) \cdot \Delta A(r_i, \Delta r, x)}{\pi r_d^2}. \quad (6.1)$$

Here, R is the length of the domain, $\Delta V(r_i, \Delta r, x)$ and $\Delta A(r_i, \Delta r, x)$ are, respectively, the volume and area of the domain receiving dose $D_{KC}\left(z_{eff}, r_i - \frac{1}{2}\Delta r, E, \mathrm{LET}\right)$, r_d is the domain radius, Δr is the step size between the different distances from the trajectory and i is the number of steps applied in the calculation. The relationship between energy and LET for each particle was found from stopping power tables. To calculate $\Delta A(r_i, \Delta r, x)$, the three cases illustrated in Figure 6.2 must be considered.

In case I, $r_i + x \leq r_d$, and here the area of the domain which receives dose $D_{KC}\left(z_{eff}, r_i - \frac{1}{2}\Delta r, E, \mathrm{LET}\right)$ is the area of a circle with radius r_i minus the area of a circle with radius $r_i - \Delta r$:

$$\Delta A(r_i, \Delta r) = \pi \cdot \left(r_i^2 - (r_i - \Delta r)^2\right). \quad (6.2)$$

In case II, $r_i + x > r_d$ and $r_i + r_d < x$, and here, the area equals the area of interception between two circles with radius r_i and r_d minus the area of interception between two circles with radius $(r_i - \Delta r)$ and r_d. The area of interception between two circles can be calculated using the following:

$$A(R_1, R_2, x) = R_1^2 \cos^{-1}\left(\frac{d^2 + R_1^2 - R_2^2}{2xR_1}\right) + R_2^2 \cos^{-1}\left(\frac{d^2 + R_2^2 - R_1^2}{2xR_2}\right) - \frac{1}{2}\sqrt{(-x + R_1 + R_2)(x + R_1 - R_2)(x - R_1 + R_2)(x + R_1 + R_2)}, \quad (6.3)$$

where R_1 and R_2 are the radii of the two circles, and x is the impact parameter (Weisstein 2003). In case III, $x \geq r_d + r_i$, and therefore larger than the maximum impact parameter where the ions can still give an energy deposition to the domain. In this case, no dose is given to the domain.

In the MKM version described in Kase *et al* (2006) and applied clinically at NIRS, the $z_{1\mathrm{D}}^*$ is given by

$$z_{1\mathrm{D}}^* = \frac{\int_0^\infty z_{\mathrm{sat}} z f_1(z)\,\mathrm{d}z}{\int_0^\infty z f_1(z)\,\mathrm{d}z}. \quad (6.4)$$

Here, $f_1(z)$ is the probability density of z deposited by a single energy-deposition event of the domain and z_{sat} represents the saturation-corrected specific energy.

When mono-energetic ion irradiation is considered, z_{sat} and z can be described as a function of the impact parameter. In this case it was shown by Inaniwa *et al* (2010) that $z^*_{1\mathrm{D}}$, for a given ion charge, LET and energy, can be generated using the following:

$$z^*_{1\mathrm{D}} = \frac{\int_0^{X_m} z_{\mathrm{sat}}(x)z(x)\cdot 2\pi x \mathrm{d}x}{\int_0^{X_m} z(x)\cdot 2\pi x \mathrm{d}x} \approx \frac{\sum_i z_{\mathrm{sat}}(x_i)z(x_i)\cdot 2\pi x_i \Delta x}{\sum_i z(x_i)\cdot 2\pi x_i \Delta x}, \tag{6.5}$$

where Δx is the size of the impact parameter steps used in the summation and X_m is the maximum impact parameter where the ions can still give an energy deposition to the domain. The function $z_{\mathrm{sat}}(x)$ is given in Appendix A in Paper III, and is a function of $z(x)$ and three constants: the domain radius (r_d), the nucleus radius (R_n), and the radiosensitivity parameter β.

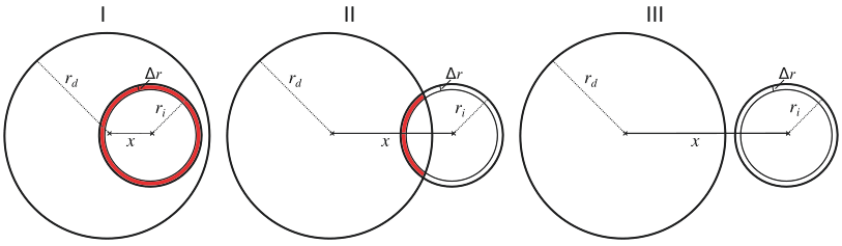

Figure 6.2: The three scenarios to account for when calculating the specific energy given by an ion to the domain with radius r_d, for a given impact parameter x: the domain will receive all dose given by the ion for this track radius r (case I), the domain will only receive part of dose from the ion (case II) and the domain will not receive any dose (case III). The part colored in red illustrates the area which receives a given dose.

6.2.2 Recalculation of carbon ion treatment plans

The carbon ion treatment plans applied in Paper II and III were originally optimized with commercial TPSs and then recalculated with different biological dose models in FLUKA. The commercial TPSs were either the NIRS TPS (applying the Kanai model) or the Syngo (VC11B, Siemens AG, Erlangen, Germany) TPS at CNAO (applying the LEM I). The treatment plans were recalculated using CNAO's in-house-made scripts for converting CT information and beam information from the original treatment plan to a format readable by FLUKA.

Treatment plans originally optimized with the Kanai model were reoptimized with the MKM in FLUKA to test the FLUKA implementation of the

MKM. While the Kanai model and the MKM differs, they both provide uniform clinical dose distributions to the targets, consistent with the dose prescription (Inaniwa *et al* 2015). These treatment plans were passively delivered plans, requiring the beam in FLUKA to be properly collimated on the patient's tumor and modulated by ridge filters to be equivalent to the plan delivered at NIRS.

Treatment plans originally optimized at CNAO were recalculated in FLUKA using an implementation (created at CNAO) of the CNAO beamline geometry in FLUKA (illustrated in Figure 6.3). In the FLUKA implementation of the CNAO beamline, the beamline is fixed, and when simulating a patient irradiated from multiple angles, the patient geometry (Figure 6.3d) is rotated and not the beamline.

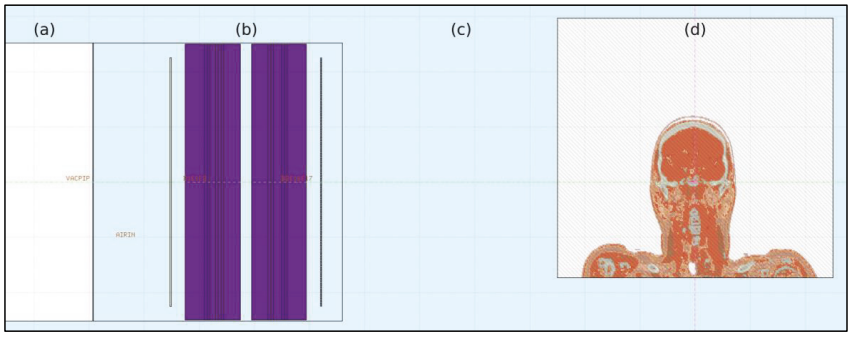

Figure 6.3: Illustration of the CNAO beamline in FLUKA, from the geometry editor in FLUKA's graphical user interface (flair): vacuum pipe (a), the two beam monitoring chambers (b), air (c) and patient structure obtained from a CT DICOM image (e).

6.3 A biological dose method accounting for hypoxia

To include cell oxygen levels, as well as the RBE, in biological dose calculations, a biological dose method based on the RBE and the OER was developed (Paper IV). The method applies an existing variable RBE model which is based on the LQ model (see Equation (3.3) in Section 3.2), and adapts the model to hypoxia by modifying the aerobic radiosensitivity parameters of the particles, α_a and β_a, to be functions of the OER:

$$\alpha_h = \frac{\alpha_a}{\mathrm{OER}(L,p)}, \tag{6.6}$$

$$\sqrt{\beta_h} = \frac{\sqrt{\beta_a}}{\mathrm{OER}(L,p)}, \tag{6.7}$$

where L is the LET_d and p is the pO_2. The OER given by the following:

$$\mathrm{OER}(L,p_h) = \frac{\sqrt{\alpha^2(L,p_h)-4\beta(p_h)\cdot\ln(S)}-\alpha(L,p_h)}{\sqrt{\alpha^2(L,p_a)-4\beta(p_a)\cdot\ln(S)}-\alpha(L,p_a)} \cdot \frac{\beta(p_a)}{\beta(p_h)}, \tag{6.8}$$

with $\alpha(L,p)$ and $\beta(p)$ defined as:

$$\alpha(L,p) = \frac{(a_1+a_2\cdot L)\cdot p+(a_3+a_4\cdot L)\cdot K}{p+K}, \tag{6.9}$$

$$\sqrt{\beta(p)} = \frac{b_1\cdot p+b_2\cdot K}{p+K}. \tag{6.10}$$

Here, *K* is a parameter which controls the rate of change in OER with pO_2 and is set to 3 mmHg and a_1, a_2, a_3, a_4, b_1 and b_2 are model parameters found by fit of *in vitro* data. The OER model was based on Wenzl & Wilkens (2011), however, with the model parameters modified to proton *in vitro* data only.

The method was implemented in FLUKA (Paper IV) and in the FLUKA based treatment planning tool (Paper V). To demonstrate model performance, SOBPs in water phantoms with pO_2 varying for strongly hypoxic (0.01 mmHg) to aerobic (30 mmHg) was applied in Paper IV, while a SOBP scenario in a water phantom with pO_2 varying with depth was applied in Paper V. The method was also demonstrated (in both Paper IV and V) on a head and neck cancer patient with pO_2 levels estimated from [^{18}F]-EF5 PET images.

6.3.1 Recalculating proton plans

Recalculation of proton treatment plans with the biological dose model accounting for hypoxia (Papers IV and V) was based on our in-house made system for recalculation of treatment plans in FLUKA, described in Section 4.2. In this system, the patient is always kept still, while the beam is rotated around it. The main modification of our in-house system was the implementation of the hypoxia adapted biological dose calculation method in FLUKA. In addition, the script for converting scored quantities into DICOM RT Dose files was modified to both store the correct biological dose and the pO_2 values in separate files, to enable plotting of both the biological dose distribution and of the patient pO_2 distribution.

The FLUKA implementation was done using the *fluscw* user routine, as with the implementation of the MKM described in Section 6.2. The difference to the MKM implementation was the description of the α and β parameters. In the hypoxia model they are functions of α_a and β_a (aerobic radiosensitivity parameters), which in proton therapy often is functions of the LET_d, and of the OER, which is a function of pO_2 and LET_d. The LET_d was estimated as described in Section 6.1.1, while the pO_2 values were implemented in FLUKA by tables connecting the particle position to pO_2, as described in the following.

6.3.2 Creating pO_2 tables

When creating the pO_2 tables for FLUKA, the first step was to estimate the pO_2 corresponding to each PET voxel. The pO_2 values were estimated from [^{18}F]-EF5 PET images, by creating a conversion curve from PET uptake to pO_2, based on PET uptake in organs with known pO_2 values (described in detail in Appendix A in Paper IV). Then, the coordinate system of the PET image was converted to the FLUKA coordinate system, based on our in-house made tool for FLUKA based treatment plan recalculation (Section 4.2). Here, isocenter of the treatment plan is the origin of the coordinate system.

The pO_2 table included information on the voxel size in each direction (Δx, Δy and Δz), and on the position of each separate voxel and its pO_2 value. In the *fluscw* routine, it is possible to obtain information on the particle position (x, y, z). Therefore, to make the table readable by *fluscw*, the starting position of each separate pO_2 voxel was described with its coordinate (x_i, y_i, z_i). Then, the *fluscw* routine could find the voxel corresponding to the particle position, by using an if-sentence corresponding to $x_i \leq x < x_i + \Delta x$, $y_i \leq y < y_i + \Delta y$ and $z_i \leq z < z_i + \Delta z$. The pO_2 value in this voxel was then assigned to the particle at this position.

6.3.3 Implementation in the FLUKA based treatment planning tool

The biological dose model accounting for hypoxia was implemented in the FLUKA based treatment planning tool, to enable optimization of treatment plans with this model (Paper V). The workflow of the FLUKA based treatment planning tool is given in Figure 6.4. First, an initial guess of the treatment plan, generally from a

commercial TPS, is recalculated in FLUKA, where αD and $\sqrt{\beta}D$ are scored. Then, the optimizer calculates the RBE according to Equation (3.3) in Section 3.2. The *fluscw* user routine from Paper IV was used to score αD and $\sqrt{\beta}D$, however, some format modifications had to be done as the optimizer runs on the FLUKA development version. Prescription dose to PTV and constraints to relevant OARs, as well as the photon radiosensitivity parameters, were given in separate files which the optimizer reads. The optimization was done using the dose difference optimization algorithm described in Mairani *et al* (2013).

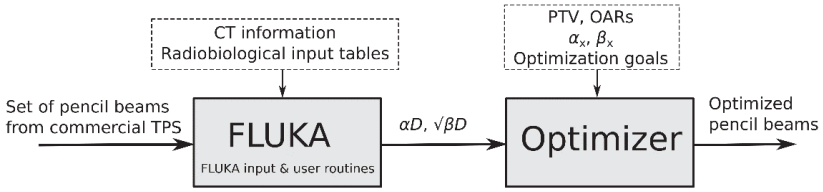

Figure 6.4: Workflow of the procedure for dose optimization with the Monte Carlo based treatment planning tool. Adapted from workflow chart by Mairani *et al* (2013).

6.4 Ethical considerations

The patient data applied in this study was provided by CNAO (Paper II and III) and Turku University Hospital (Paper IV and V) and was used with permission from these facilities. All patient material was anonymized, and the patients from Turku University Hospital were part of a study registered at ClinTrials.Gov under No. NCT 01774760.

7. Summary of Results

7.1 More accurate knowledge of the LET for cell experiments

7.1.1 Paper I: LET estimations at cell irradiation positions at the OCL

In Paper I, the experimental setup for cell irradiation at the Oslo Cyclotron Laboratory (OCL) was implemented in the FLUKA Monte Carlo (MC) code. Comparisons between FLUKA simulated dose and measured dose data at three potential cell irradiation positions showed that the experiment was carried out with a 15.5 MeV proton beam. A MC simulated 80 MeV proton beam (representing a low-energy proton beam at clinical facilities) was included for comparisons.

The OCL LET_d were found to increase from 4-7 keV/µm at the beam entrance to 34-35 keV/µm at the proton range, R_{80} (Figure 7.1a). This was significantly higher than the 80 MeV proton beam LET_d, which was less than 15 keV/µm at the proton range. The LET spectra broadened with beam depth (Figure 7.1b). However, the OCL LET spectra were still considerably narrower than the 80 MeV proton beam spectra which resulted in the same LET_d values. The setup can therefore be used to study the RBE-LET relationship of protons with narrow LET spectra and high LET_d values. However, as the LET_d varies rapidly at these energies, accurate dosimetry and MC simulations are essential for reducing uncertainties.

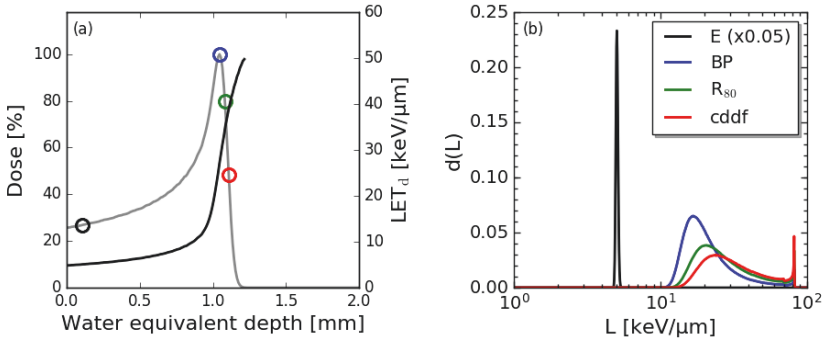

Figure 7.1: Depth dose profile (gray) of the OCL proton beam with corresponding LET_d (black) (a) and LET spectra (b), estimated at one of the cell irradiation positions. The LET spectra were estimated at the beam entrance, E (black), Bragg peak, BP (blue), particle range, R_{80} (green) and center of distal dose fall-off, cddf (red), as illustrated by circles in (a). The figure is reprinted from Paper I with permission from Taylor & Francis Group.

7.2 Study of a clinical RBE model

7.2.1 Paper II: Implementation of the MKM in FLUKA

In Paper II, the RBE model used for carbon ion therapy at NIRS in Japan (the MKM) was implemented in FLUKA. The MKM is based on the saturation-corrected dose-mean specific energy (z_{1D}^{*}) to small subvolumes of the cell nucleus called domains. Calculations of specific energy and z_{1D}^{*} were in good agreement with the calculations applied at NIRS (Figure 7.2). Small differences in the calculated z_{1D}^{*} were observed for helium ions at low energies, resulting from the choice of energy versus LET input table, as the accuracy of these tables depends on how they are estimated. However, the observed differences were shown to not affect agreements with experimental data at clinically relevant energies.

Comparisons between carbon ion biological dose calculations performed using the FLUKA implementation and the NIRS TPS showed a satisfactorily agreement, with median target RBE deviations of at most 3% for the applied patient cases (prostate and pancreas). Larger differences were observed for RBE values registered for small portions of the target volume. However, these differences were still small enough to be attributed to differences between the MC detailed particle transport and the analytical method of the TPS. The implementation enables direct comparisons in FLUKA between the biological doses estimated using the LEM and the MKM for given treatment scenarios.

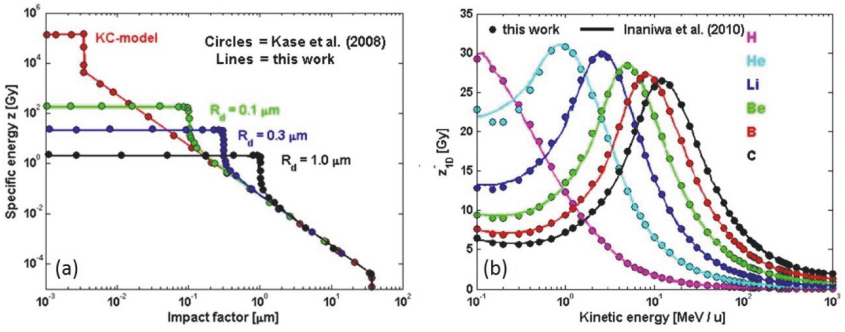

Figure 7.2: Comparison between our calculations and calculations from NIRS: the specific energy, z, as a function of impact parameter (a) and the saturation-corrected dose-mean specific energy, z_{1D}^{*}, as a function of kinetic energy for six ion types (hydrogen to carbon). The figure is reprinted from Paper II with permission from IOP Publishing.

7.2.2 Paper III: Sensitivity study of the MKM model parameters

A sensitivity study of the MKM was performed in Paper III, to assess potential under- or over-dosage of a tumor and surrounding healthy tissue due to errors in the model parameters. Variations in the domain radius, r_d, had the largest impact on the biological dose estimations, as seen in Figure 7.3 for a carbon ion SOBP in water. This was not surprising, as r_d represents the sensitive volume in the MKM, and the estimated specific energy is highly dependent on the size of this volume. Variations in the nucleus radius, R_n, resulted mainly in changes in the biological dose toward the particle range. This was because R_n is only used in the saturation correction at high specific energy regions, found at the distal end of the beam. Variations in the radiosensitivity parameters α_x and β resulted in small and almost reverse changes in the biological dose. Generally, the relative changes in the biological dose were less than the percentage change of the parameter.

The carbon ion SOBP in water was also recalculated applying the MKM with input parameters based on V79, T1 and CHO cells. This gave mostly higher biological doses than the HSG SOBPs, with a few exceptions at the beam entrance. While the parameter sets differed significantly, the combined effect of each parameter set resulted in moderate differences across calculated biological doses. Also, while an increase in biological dose was observed towards the particle range for the V79, T1 and CHO calculated SOBPs, all parameter sets resulted in a flat SOBP when two opposing beams were combined. A clinical case (clivus chordoma tumor) showed the same dependencies on parameters as the SOBPs in water.

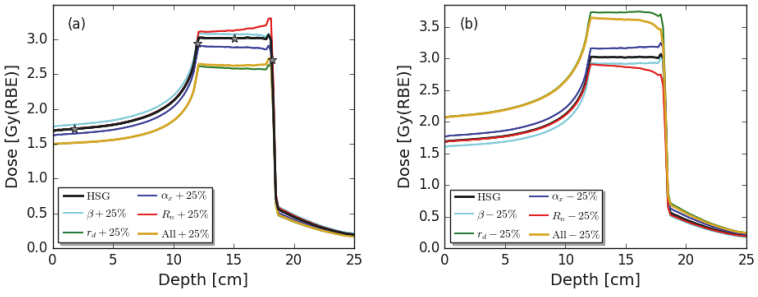

Figure 7.3: Depth dose profiles in water for a 3 Gy(RBE) carbon ion SOBP, optimized with nominal HSG parameters and recalculated with HSG parameters increased (a) and decreased (b) separately by 25 %, respectively. The figure is reprinted from Paper III with permission from IOP Publishing.

7.3 Including hypoxia in biological dose calculations

7.3.1 Paper IV: Development and implementation of a hypoxia model in FLUKA

A biological dose calculation method which accounts for hypoxia and RBE was developed for proton therapy and implemented in FLUKA in Paper IV. The biological dose decreased with decreasing pO_2 values, similar to the respective OER, both when applying an RBE of 1.1 ($D_{RBE1.1}$) and the variable RBE model by Rørvik *et al* (2017) (D_{ROR}). The OER was mostly constant throughout the beam, with a slight decrease at high LET_d. This decrease was most prominent at low oxygen levels; at the most extreme hypoxic condition applied in the study (0.01 mmHg) the OER value went from 2.7 at the beam entrance to 2.3 at the distal end of the beam.

The pO_2 values on a voxel-by-voxel basis in a head and neck cancer patient were estimated from [^{18}F]-EF5 PET images, showing areas with low pO_2 in the PTV. At the corresponding locations, the biological dose was lower than the prescribed dose, as illustrated in Figure 7.4. The PTV had pO_2 values in the range of 2.2 - 60 mmHg, with mean pO_2 of 16.8 mmHg. The resulting median target biological doses calculated using $D_{OER,RBE1.1}$ and $D_{OER,ROR}$ was a factor 1.12 and 1.11 lower than the $D_{RBE1.1}$ and D_{ROR} biological doses, respectively. This corresponds well with the OER at 16.8 mmHg for low-LET radiation. The results show that neglecting the effect of hypoxia in proton therapy could potentially compromise the expected tumor control probability and should, together with RBE variations, therefore be kept in mind in clinical practice.

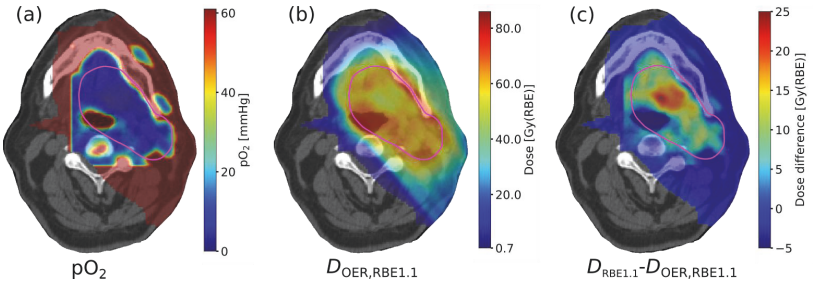

Figure 7.4: Head and neck cancer patient; pO_2 map (a), $D_{OER,RBE1.1}$ biological dose (b) and dose difference between $D_{RBE1.1}$ and $D_{OER,RBE1.1}$ biological doses (c). The PTV is delineated in pink. The pO_2 table includes only pO_2 values inside and directly around the PTV, while outside the table the pO_2 was set to 60 mmHg. The pO_2 in voxels receiving doses below 0.7 Gy(RBE) according to the $D_{RBE1.1}$ dose is set transparent.

7.3.2 Paper V: Optimization of treatment plans with the hypoxia model

In Paper V, the hypoxia model from Paper IV was implemented in a FLUKA based treatment planning tool. The tool was demonstrated on two proton SOBP scenarios (single and opposing fields) in a simulated water phantom and for the head and neck cancer patient from Paper IV. The water phantom had pO_2 levels varying with depth in the beam direction. Optimization of the SOBP scenarios in water resulted in similar dose distributions, with a nearly homogeneous biological dose distribution to the target (Figure 7.5) in both cases. The corresponding RBE distribution (where only the proton dose accounts for hypoxia) were seen to follow the oxygen levels almost in a stepwise manner. The RBE in the most hypoxic region (2.5 mmHg) was a factor of 1.43 below the RBE of 1.1 at non-hypoxic regions. This is close to the OER at 2.5 mmHg for low-LET radiation.

The patient pO_2 was estimated from [^{18}F]-EF5 PET images. The patient plan was reoptimized with the hypoxia model, resulting in a median PTV dose of 70.8 Gy(RBE), agreeing satisfactorily with the prescribed dose of 70 Gy(RBE). However, the dose to one of the parotid glands was increased considerably compared to the original Eclipse optimized treatment plan which did not account for hypoxia. Still, as the contra-lateral parotid gland was almost completely spared, the probability of xerostomia (dry mouth) would be small for this case. Taking account of the RBE and OER in biological dose optimization can give a more beneficial physical dose distribution to the tumor, however, it may lead to violation of normal tissue constraints.

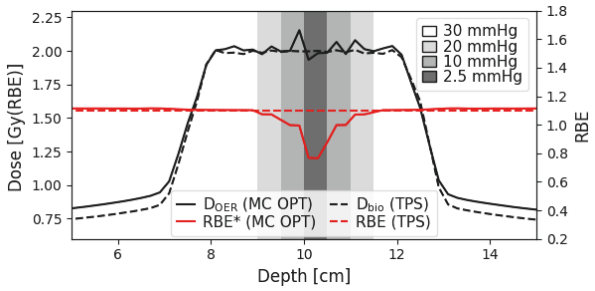

Figure 7.5: Biological dose distributions (black) optimized with the Monte Carlo based optimizer (MC OPT) using the hypoxia model (solid line) and with the Eclipse TPS using a constant RBE of 1.1 (dashed line), with corresponding RBE distributions (red). *The MC OPT RBE is not a directly an RBE distribution, as only the proton parameters accounts for hypoxia and not the photon parameters.

8. Discussion

The RBE is currently applied in treatment planning in particle therapy to account for the different biological effectiveness across radiation qualities. This makes it possible to use treatment protocols from conventional radiotherapy (or from earlier clinical experience with particles) in particle therapy. It also makes it possible in treatment planning to optimize a homogeneous biological dose to the target, as done in clinical carbon ion therapy. The accuracy of the estimated RBE is therefore important for the treatment received by particle therapy patients. In this thesis, the RBE and biological dose has been studied using the FLUKA Monte Carlo code. Initially, a cell irradiation experiment was implemented in FLUKA to enable accurate dose and LET estimates in the cell irradiation positions (Paper I). In the next project, the RBE model applied clinically in Japan (the MKM) was implemented in FLUKA (Paper II), and further investigated through a sensitivity study of the model input parameters (Paper III). Finally, a biological dose method which accounts for hypoxia and RBE was developed and implemented in FLUKA (Paper IV) and in a FLUKA based treatment planning tool Paper V).

Monte Carlo simulations are useful in particle therapy, as they can provide additional and more accurate information on how the radiation interact in tissue compared to analytical treatment planning systems. The physics models of FLUKA have been shown to reproduce measured depth and lateral dose profiles in water well for all clinically interesting ions. They have, in addition, been shown to treat the transport and interaction of primary particles and produced fragments consistently for protons and ion beams at therapeutic energies (Battistoni *et al* 2016). FLUKA is applied at the leading European particle therapy centers CNAO and Heidelberg Ion-beam Therapy Center (HIT), both in research and to guide treatment planning decisions when needed (Parodi *et al* 2012, Tessonnier *et al* 2014). FLUKA has also been used to support developments of some commercial analytical TPSs (Battistoni *et al* 2016). FLUKA may therefore be a helpful tool when we get our first proton centers to Norway in a few years.

8.1 Improving RBE measurement data

While a constant RBE of 1.1 is currently applied clinically in proton therapy, it is becoming widely accepted that the proton RBE is variable and that proton therapy could benefit from including a variable RBE in treatment planning (Willers *et al* 2018). However, the currently existing proton RBE models estimate considerable different RBE values, complicating the introduction of variable RBE in clinical proton therapy (Rørvik *et al* 2018). In carbon ion therapy, the RBE varies significantly and must be accounted for clinically. However, the clinically applied carbon ion RBE models estimate vastly different biological dose distributions for the same irradiation scenarios. Better RBE data are therefore required to increase the accuracy of the RBE estimates, both for proton and carbon ion therapy. The aim of Paper I was to improve *in vitro* RBE data for protons. This was done by providing an accurate description of the dose and (in particular) the LET distribution in a cell irradiation experiment, which subsequently has been used in several cell irradiation studies (Rykkelid 2017, Baker 2018, Tormodsrud 2019).

In proton RBE models, the LET is commonly described by the LET_d (Rørvik *et al* 2018). While there is currently an abundance of *in vitro* RBE-LET data which can be used for RBE models, the data are associated with large uncertainties (Paganetti 2014). Most published *in vitro* RBE experiments do not provide the LET_d at the measurement points, and when it has been reported it is often roughly estimated from stopping power tables, based on the beam energy (Paganetti 2014). To ensure accurate LET estimations of the beam, it is therefore important with proper implementation of the experimental setup in Monte Carlo codes (Durante *et al* 2019). This was also emphasized in an editorial following the publication of Paper I (Grassberger and Paganetti 2017), which highlighted how Paper I and similar studies are necessary in paving the way for clinically biological treatment modelling, by decreasing experimental error by characterizing the incoming beam properly.

In addition to having a proper implementation of the experimental setup, it is important to report how the LET values were calculated, as this influences the

estimated values. In this thesis, the LET_d and LET spectra have been estimated based on primary and secondary protons only, which has also been typical in other studies (Yepes *et al* 2019, Granville and Sawakuchi 2015). Grassberger and Paganetti (2011) showed that secondary protons have a significant influence on the clinical LET_d distribution and should therefore be included in biological optimization. Including other secondary particles may also have a significant impact on the LET_d estimation and can even double the LET_d value (Grzanka *et al* 2018). Another difference in reported LET values arises from whether the LET to water or to tissue is estimated, as these can differ significantly (Wilkens and Oelfke 2004). In this thesis, the LET to water was scored, as dose to water is the standard to report in radiotherapy (IAEA 2000). The LET can also be scored volumetrically or across the boundary of two regions (Guan *et al* 2015). The LET_d was, in this thesis, scored volumetrically, in a grid equal to the dose grid, while the LET spectra were scored across boundaries. The LET_d could also be scored across boundaries, however, this method has some limitations when scoring the LET_d from irradiation scenarios with several beams.

Most variable RBE models for protons are, as mentioned, based on the LET_d. However, when comparing the low-energy OCL proton beam with an 80 MeV proton beam (Paper I), significantly different LET spectra were observed for the same LET_d values. Similar results were found by Howard *et al* (2018), who compared a 71 MeV proton beam and a 160 MeV proton beam, and observed clear differences in lineal energy spectra for the same dose-averaged lineal energy. Also, it can be shown that estimating the RBE from the LET_d is only appropriate if the relationship between the RBE and LET is linear. This emphasizes the hypothesis in Rørvik *et al* (2017) that proton RBE models based on the LET spectrum may be more appropriate than models based on the LET_d. Grün *et al* (2019) further showed that the RBE can only be accurately reflected by the LET_d for narrow LET distributions. If the inaccuracy of using the LET_d for expressing the RBE in a mixed field is large enough to be clinically relevant, it should be studied further. However, only full Monte Carlo software like FLUKA is currently able to produce the full LET

spectra of a beam. To implement an RBE model based on the LET spectrum in a commercial TPS, an analytical algorithm for the full LET spectrum must therefore be created, unless the commercial TPS is MC based. Similar considerations might also be relevant in carbon ion therapy, where the RBE is often characterized by the frequency or dose mean values of the specific energy (Grün *et al* 2019).

While LET is the most widely used quantity describing the radiation quality, microdosimetric quantities may be more accurate to use, as these will reflect the statistical nature and the spatial patterns of energy depositions in the ion track (Liamsuwan *et al* 2014). Microdosimetric quantities may also, unlike the LET, be measured directly in the beam. However, applying microscopic quantities presents some challenges. Liamsuwan *et al* (2014) showed that the dose-averaged lineal energy (y_{d}) depended to a large degree on the target size, with decreasing y_{d} with increasing target size. This was also observed in our sensitivity study in Paper III, where the radius of the domain had a large impact on the estimated saturation-corrected dose-mean specific energy.

RBE models are generally based on *in vitro* data. However, the radiosensitivity of cell lines might not reflect a clinical scenario perfectly. Studies on *in vivo* and clinical RBE should therefore give a more realistic picture of the RBE in a clinical beam. However, there are only a limited number of such studies (Sørensen *et al* 2017). To better utilize existing *in vivo* RBE data, Lühr *et al* (2017) introduced a beam quality factor Q, as an alternative to the LET, to quantify the RBE. By applying Q, which is a function of the charge and energy of the ion, in RBE estimates, the RBE dependency on ions which exists with the LET can be removed. This makes it possible to utilize *in vivo* data for heavier particles when determining the proton RBE.

A few years ago, there was still no clinical evidence suggesting that the proton RBE deviated significantly from the applied value of 1.1 (Paganetti 2015). However, several newer *in vivo* studies have shown that the RBE of 1.1 is most likely an underestimation (Sørensen *et al* 2017, Saager *et al* 2018). Recent studies have also found clinical evidence that support a variable RBE. Peeler *et al* (2016)

showed that changes on post treatment MR images in children treated with proton therapy depended on both the physical dose and the LET, and a study on chest-wall patients by Underwood *et al* (2018) supports the hypothesis of a variable clinical proton RBE. Eulitz *et al* (2019) further studied post MR images in four glioma patients treated with proton therapy and showed that non-uniform distributions of necrotic lesions within the brain were highly correlated with a combination of dose and LET.

8.2 Applying variable RBE models clinically

Variable RBE models are currently applied clinically in carbon ion therapy, with the leading models being the LEM I in Europe and the MKM in Japan. These models estimate significantly different RBE values for the same scenarios (see Figure 4.1 in Section 4.3), and carbon ion treatment protocols can therefore not be directly interchanged between European and Japanese facilities. It is therefore of high clinical relevance to have the possibility of making direct comparisons between the two models. This was the goal of Paper II, and was achieved by implementing the MKM in FLUKA, where the LEM had already been implemented (Mairani *et al* 2010). The significant differences between the models also make it relevant to assess possible uncertainties in the models, which was conducted in Paper III.

While the MKM and LEM I estimate significantly different biological dose distributions, they are based on some conceptual similarities. In both models the main target is the cell nucleus, which is divided into small independent subvolumes. Also, the summation of the local effect in these subvolumes determines the cell survival probability in both models (Kase *et al* 2008). However, the size of the subvolumes and the dose-effect curves are different between the models (Kase *et al* 2008). The endpoint of the applied clinical models also differs; the clinical MKM uses parameters based on HSG cells while the clinical LEM uses a general $(\alpha/\beta)_x$ of 2 Gy (Fossati *et al* 2012). The MKM applied at NIRS also uses a carbon ion beam as reference radiation, and not photons as used in LEM.

Japan has the longest clinical experience in carbon ion therapy. While the originally applied Kanai model (Kanai *et al* 1999) included many simplifications, its

appropriateness was demonstrated by the observed local tumor control (Inaniwa *et al* 2015). To make use of this experience, CNAO in Italy adapt their clinical protocols to Japanese protocols by applying conversion factors (target median dose ratios). These factors were estimated by Fossati *et al* (2012) and later confirmed by Molinelli *et al* (2016), and are computed as median target ratios. While the conversion factors are based on the Kanai model, the target dose is the same with the Kanai model and the clinically applied MKM model. However, as seen earlier (Figure 4.1 in Section 4.3 and Paper II), the difference between the LEM I and the MKM or Kanai model is not only a generic scaling difference. Applying scaling factors to convert normal tissue constraints between the facilities may therefore be a problem. Dale *et al* (2019) showed that the dose constraints applied for the optic nerve at CNAO, based on NIRS constraints, are conservative, and they proposed new and safe dose constraints for this OAR. They also stressed the need for validation of OAR constraints for both RBE models. Having the FLUKA tool available for recalculating treatment plans with both LEM I and MKM (Paper II) is therefore useful, as it can provide exact dose distributions for comparisons.

The LEM has been further developed several times, with LEM IV being the newest model version. The main concept of the LEM, i.e. equal local dose should result in equal biological effect, is conserved in the LEM IV (Elsässer *et al* 2010). However, in the LEM IV, the biological response is directly related to the double-strand break pattern (Giovannini *et al* 2016). The LEM IV has a stronger dependence on the LET than the LEM I, and studies suggests that the LEM I is best at predicting the RBE at low-LET regions, while the LEM IV is most accurate in high-LET regions (Karger and Peschke 2018, Saager *et al* 2018). However, as there are currently not enough data to assess whether the LEM I or the LEM IV is best at describing clinical scenarios, the LEM I is still applied clinically in Europe (Gillmann *et al* 2019).

The large differences in the biological dose estimates between the various models enhances the importance of assessing the model uncertainties. The purpose of Paper III was therefore to study how uncertainties in the MKM input

parameters (domain radius, nucleus radius, α_x and β) would impact the biological dose. This has been done partly for the LEM I (Chanrion *et al* 2014), and more comprehensively for the LEM IV (Böhlen *et al* 2012, Friedrich *et al* 2013b). For the MKM, however, only less extensive sensitivity studies had been performed (Remmes *et al* 2012, Mairani *et al* 2017). The sensitivity study in Paper III showed that uncertainties in the domain radius resulted in the greatest uncertainties in the MKM biological dose, with decreasing biological dose with increasing domain radius. Böhlen *et al* (2012) found for the LEM IV that the largest risk of misestimating was expected in the high-LET area inside and close to the PTV. The same was observed in Paper III when varying the entire MKM parameter sets. Friedrich *et al* (2013b) found, similar to us, that a change in model parameters (in this case the LEM IV parameters) resulted in a smaller percentage change in the resulting RBE. To further reduce uncertainties, Friedrich *et al* (2013b) suggested using for instance biomarkers for a more personalized determination of input parameters.

In proton therapy treatment planning, variable RBE is, as already mentioned, not yet implemented clinically. However, there is an awareness of the potential RBE issues during treatment, especially the fact that the RBE increases with increasing depth in patient. This is currently handled by careful selection of field angles, avoiding organs at risk at the distal end of the treatment fields (Paganetti *et al* 2019). However, there is a growing consensus in the scientific community that these measures are insufficient, and that incorporation of more detailed RBE parameters in proton therapy treatment planning is a necessary step to improve the quality of the treatment (Willers *et al* 2018). Currently at the MD Anderson Cancer Center in Texas, USA, the first clinical trial worldwide which includes variable RBE in proton therapy treatment planning is initiated (MD Anderson Cancer Center 2019). While this clinical trial only includes a relatively simple RBE model (LET optimization), it is a step in the direction towards including variable RBE in proton therapy.

8.3 Including hypoxia in biological dose calculations

Hypoxia relates to poor treatment prognosis and outcome. This poses a significant problem in cancer treatment, as studies show that most types of solid tumors contains hypoxic regions of clinical significance (Dhani *et al* 2015, Evans *et al* 2009). Tumor hypoxia varies on a tumor-to-tumor basis, and the presence and extent of hypoxia must therefore be assessed in each patient to optimize the treatment (Koch and Evans 2015). Paper IV and V addressed this issue, by first developing a biological dose method adapted for hypoxia, and then by creating tools for recalculating and optimizing proton treatment plans with this method. The tools showed promising results, however, better estimation of the patient pO_2 is required before applying the method clinically. Also, applying the method on more patients will be needed to demonstrate the robustness of the method.

The feasibility of imaging hypoxia with PET has been clinically demonstrated in several cancer types (Kelada and Carlson 2014). Applying imaging modalities like PET and magnetic resonance imaging (MRI) for estimating hypoxia is non-invasive and feasible in a clinical setting. Several PET hypoxia tracers have already been used in completed or ongoing clinical trials on simultaneous dose escalation using a dose painting technique in photon therapy (Zhang et al 2016). However, it has been shown that the detection of hypoxia is still imperfect, and that the focus on hypoxia detection should continue (Bredell *et al* 2016). In the process of assessing how accurate the modalities are at estimating hypoxia, it could be interesting to compare different image modalities, like different PET tracers (e.g. [^{18}F]-EF5, [^{18}F]-FMISO and [^{18}F]-FDG) and different techniques of MRI (e.g. DCE-MR and DSC-MR). Detecting hypoxia only prior to treatment may also be insufficient, as the extent of hypoxia in the tumor will vary during treatment. However, as the treatment will most likely reduce the hypoxic region, it will still be beneficial to include hypoxia information from before treatment in the treatment plans (Lin *et al* 2008).

Methods proposed for overcoming hypoxia during radiotherapy treatment is, as mentioned in Section 3.3, dose painting, LET painting and including the OER in biological dose calculations (as done in Paper IV and V). The last method has the

benefit of also having the possibility of directly including a variable RBE in the calculations. To quantify which method is best, tumor control probability (TCP) models and normal tissue complication probability models can be applied, as these types of models are commonly used to assess the outcome of radiotherapy (McNamara *et al* 2019). Malinen and Søvik (2015) estimated the TCP of dose and LET painting for protons, lithium ions and carbon ions and concluded that the clinical impact of LET painting was smaller than that of dose painting. Also, while combined dose and LET painting gave the highest TCPs overall, the increased effect was not substantial compared to dose painting alone.

The OER decreases with increasing RBE, and carbon ions are therefore more effective in killing hypoxic tumors than protons and photons. Dose painting has therefore less of an effect in carbon ion therapy than proton therapy, as carbon ions are already quite effective without dose painting. This was observed by Malinen and Søvik (2015), and they also saw that LET painting had larger effect with carbon ions than protons. As the OER of carbon ions are lower than that of low-LET radiation like photons, the carbon RBE will be increased in hypoxic regions. The hypoxia tools created in Paper IV and V may be useful for further exploration of the potential of protons and carbon ions in treatment of hypoxic tumors.

9. Conclusions

Particle therapy is an established alternative to conventional radiotherapy for many cancer types, with dosimetric advantages which makes it possible to better confine the dose to the tumor. However, uncertainties in the RBE and biological dose is a limitation which must be reduced for particle therapy to reach its full potential.

By decreasing the uncertainties in *in vitro* RBE data, more accurate RBE models can be obtained. The Monte Carlo simulations of the OCL experiment showed a steep increase of LET_d values around the Bragg peak, combined with steep dose gradients. This demonstrates that high spatial and dosimetric precision, obtained through accurate implementation of the beamline in a Monte Carlo code, is essential for correct assessment of the LET_d during cell irradiation experiments.

The implementation of the MKM in FLUKA has made direct comparisons of different RBE models possible. Having the possibility of direct comparisons between European and Japanese carbon ion dose distributions is beneficial when comparing clinical protocols. While uncertainties in the biological dose estimates are high, as shown by the significantly different dose distributions estimated by the models, uncertainties in the MKM parameters was shown to have a smaller impact on the estimated dose than the percentage uncertainty in the parameters.

A biological dose calculation method which accounts for both the OER and the RBE was developed and implemented in FLUKA and in a FLUKA based treatment planning tool. Underdosage of the tumor volume was seen when not accounting for hypoxia. However, optimization of treatment plans with the hypoxia model showed good potential for treatment planning, with the median target dose equal to the prescription dose and with increased physical dose in hypoxic regions.

Overall, this thesis has contributed to the knowledge on the RBE and biological dose calculations in proton and carbon ion therapy. With the increase in particle therapy facilities worldwide, including the upcoming startup of two Norwegian proton centers, improving the accuracy of RBE and biological dose calculations is more relevant than ever.

References

Baker A 2018 *In Vitro Cell Irradiation with Low Energy Protons. DNA Double Strand Break Induction and Repair Kinetics in Human Glioblastoma Cells.* (Master thesis, University of Oslo) Online: https://www.duo.uio.no/handle/10852/64902

Bassler N, Toftegaard J, Lühr A, Sorensen B S, Scifoni E, Krämer M, Jäkel O, Mortensen L S, Overgaard J and Petersen J B 2014 LET-painting increases tumour control probability in hypoxic tumours *Acta Oncol. (Madr).* **53** 25–32

Battistoni G, Bauer J, Böhlen T T, Cerutti F, Chin M P W, Dos Santos Augusto R, Ferrari A, Ortega P G, Kozłowska W, Magro G, Mairani A, Parodi K, Sala P R, Schoofs P, Tessonnier T and Vlachoudis V 2016 The FLUKA Code: An Accurate Simulation Tool for Particle Therapy *Front. Oncol.* **6** 116

Becquerel H 1896 Sur les radiations émises par phosphorescence *Compt. Rend. Acad. Sci.* **122** 420–1

Belli M, Cera F, Cherubini R, Dalla Vecchia M, Haque A M I, Ianzini F, Moschini G, Sapora O, Simone G, Tabocchini M A and Tiveron P 1998 RBE-LET relationships for cell inactivation and mutation induced by low energy protons in V79 cells : further results at the LNL facility *Int. J. Radiat. Biol.* **74** 501–9

Böhlen T T, Brons S, Dosanjh M, Ferrari A, Fossati P, Haberer T, Patera V and Mairani A 2012 Investigating the robustness of ion beam therapy treatment plans to uncertainties in biological treatment parameters. *Phys. Med. Biol.* **57** 7983–8004

Böhlen T T, Cerutti F, Chin M P W W, Fassò A, Ferrari A, Ortega P G, Mairani A, Sala P R, Smirnov G and Vlachoudis V 2014 The FLUKA Code: Developments and challenges for high energy and medical applications *Nucl. Data Sheets* **120** 211–4

Bopp C, Hirayama R, Inaniwa T, Kitagawa A and Noda K 2016 Adaptation of the microdosimetric kinetic model to hypoxia *Phys. Med. Biol.* **61** 7586–99

Bragg W H and Kleeman R 1904 LXXIV. On the ionization curves of radium *London, Edinburgh, Dublin Philos. Mag. J. Sci.* **8** 726–38

Bredell M G, Ernst J, El-Kochairi I, Dahlem Y, Ikenberg K and Schumann D M 2016 Current relevance of hypoxia in head and neck cancer *Oncotarget* **7** 50781–804

Burnet N G, Thomas S J, Burton K E and Jefferies S J 2004 Defining the tumour and target volumes for radiotherapy *Cancer Imaging* **4** 153–61

Castro J R, Quivey J M, Lyman J T, Chen G T Y, Phillips T L, Tobias C A and Alpen E L 1980 Current status of clinical particle radiotherapy at Lawrence Berkeley laboratory *Cancer* **46** 633–41

Chanrion M, Sauerwein W, Jelen U, Wittig A, Engenhart-Cabillic R and Beuve M 2014 The influence of the local effect model parameters on the prediction of the tumor control probability for prostate cancer. *Phys. Med. Biol.* **59** 3019–40

Chatterjee A and Schaefer H J 1976 Microdosimetric structure of heavy ion tracks in tissue. *Radiat. Environ. Biophys.* **13** 215–27

Curie E 1950 Marie and Pierre Curie and the discovery of radium *Br. J. Radiol.* **23** 409–12

Dale J E, Molinelli S, Vitolo V, Vischioni B, Bonora M, Magro G, Pettersen H E S, Mairani A, Hasegawa A, Dahl O, Valvo F and Fossati P 2019 Optic nerve constraints for carbon ion RT at CNAO – Reporting and relating outcome to European and Japanese RBE *Radiother. Oncol.* **140** 175–81

Dhani N, Fyles A, Hedley D and Milosevic M 2015 The clinical significance of hypoxia in human cancers *Semin. Nucl. Med.* **45** 110–21

Durante M, Orecchia R and Loeffler J S 2017 Charged-particle therapy in cancer: Clinical uses and future perspectives *Nat. Rev. Clin. Oncol.* **14** 483–95

Durante M and Paganetti H 2016 Nuclear physics in particle therapy: A review *Reports Prog. Phys.* **79** 96702

Durante M, Paganetti H, Pompos A, Kry S F, Wu X and Grosshans D R 2019 Report of a National Cancer Institute special panel: Characterization of the physical parameters of particle beams for biological research *Med. Phys.* **46** e37–52

Elsässer T, Weyrather W K, Friedrich T, Durante M, Iancu G, Krämer M, Kragl G, Brons S, Winter M, Weber K J and Scholz M 2010 Quantification of the relative biological effectiveness for ion beam radiotherapy: Direct experimental comparison of proton and carbon ion beams and a novel approach for treatment planning *Int. J. Radiat. Oncol. Biol. Phys.* **78** 1177–83

Eulitz J, Lutz B, Wohlfahrt P, Dutz A, Enghardt W, Karpowitz C, Krause M, Troost E G C and Lühr A 2019 A Monte Carlo based radiation response modelling framework to assess variability of clinical RBE in proton therapy *Phys. Med. Biol.* **64** 225020

Evans S M, Du K L, Chalian A a, Mick R, J P, Hahn S M, Quon H, Lustig R, Weinstein G S and Koch C J 2009 Patterns and Levels of Hypoxia in Head and Neck Squamous Cell Carcinomas and their relationship to Patient Outcome *Int. J. Radiat. Oncol. Biol. Phys.* **69** 1024–31

Fano U 1953 Degradation and Range Straggling of High-Energy Radiations* *Phys. Rev.* **92** 328

Ferrari A, Sala R, Fasso A and Ranft J 2005 FLUKA: a multi-particle transport code *INFN/TC* **5** 31–49

Filipak M 2012 Comparison of dose profiles for proton v. x-ray radiotherapy *Wikimedia Commons* Online: https://commons.wikimedia.org/w/index.php?curid=27983203

Fjæra L F, Li Z, Ytre-Hauge K S, Muren L P, Indelicato D J, Lassen-Ramshad Y, Engeseth G M, Brydøy M, Mairani A, Flampouri S, Dahl O and Stokkevåg C H 2017 Linear energy transfer distributions in the brainstem depending on tumour location in intensity-modulated proton therapy of paediatric cancer *Acta Oncol. (Madr).* **56** 763–8

Fleming I N, Manavaki R, Blower P J, West C, Williams K J, Harris A L, Domarkas J, Lord S, Baldry C and Gilbert F J 2015 Imaging tumour hypoxia with positron emission tomography *Br. J. Cancer* **112** 238–50

Fossati P, Matsufuji N, Kamada T and Karger C P 2018 Radiobiological issues in prospective carbon ion therapy trials *Med. Phys.* **45** e1096–110

Fossati P, Molinelli S, Matsufuji N, Ciocca M, Mirandola A, Mairani A, Mizoe J, Hasegawa A, Imai R, Kamada T, Orecchia R and Tsujii H 2012 Dose prescription in carbon ion radiotherapy: a planning study to compare NIRS and LEM approaches with a clinically-oriented strategy *Phys. Med. Biol.* **57** 7543–54

Friedrich T, Durante M and Scholz M 2013a The Local Effect Model (LEM): Basics and applications *Heal. Risks Extraterr. Environ.*

Friedrich T, Grün R, Scholz U, Elsässer T, Durante M and Scholz M 2013b Sensitivity analysis of the relative biological effectiveness predicted by the local effect model *Phys. Med. Biol.* **58** 6827–49

Gillmann C, Jäkel O and Karger C P 2019 RBE-weighted doses in target volumes of chordoma and chondrosarcoma patients treated with carbon ion radiotherapy: Comparison of local effect models I and IV *Radiother. Oncol.*

Giovannini G, Böhlen T, Cabal G, Bauer J, Tessonnier T, Frey K, Debus J, Mairani A and Parodi K 2016 Variable RBE in proton therapy: Comparison of different model predictions and their influence on clinical-like scenarios *Radiat. Oncol.* **11** 68

Gottschalk B 2016 Physics of Proton Interactions in Matter *Proton therapy physics* ed H Paganetti (CRC Press) pp 19–59

Granville D A and Sawakuchi G O 2015 Comparison of linear energy transfer scoring techniques in Monte Carlo simulations of proton beams *Phys. Med. Biol.* **60** N283

Grassberger C and Paganetti H 2011 Elevated LET components in clinical proton beams *Phys. Med. Biol.* **56** 6677–91

Grassberger C and Paganetti H 2017 Varying relative biological effectiveness in proton therapy: knowledge gaps versus clinical significance *Acta Oncol. (Madr).* **56** 761–2

Grün R, Friedrich T, Traneus E and Scholz M 2019 Is the dose-averaged LET a reliable predictor for the relative biological effectiveness? *Med. Phys.* **46** 1064–74

Grzanka L 2014 Modelling beam transport and biological effectiveness to develop treatment planning for ion beam radiotherapy *arXiv* Online: http://arxiv.org/abs/1410.1378

Grzanka L, Ardenfors O and Bassler N 2018 Monte carlo simulations of spatial let distributions in clinical proton beams *Radiat. Prot. Dosimetry* **180** 296–9

Guan F, Peeler C, Bronk L, Geng C, Taleei R, Randeniya S, Ge S, Mirkovic D, Grosshans D, Mohan R and Titt U 2015 Analysis of the track- and dose-averaged LET and LET spectra in proton therapy using the GEANT4 Monte Carlo code. *Med. Phys.* **42** 6234

Gunzert-Marx K, Iwase H, Schardt D and Simon R S 2008 Secondary beam fragments produced by 200 MeV u^{-1} ^{12}C ions in water and their dose contributions in carbon ion radiotherapy *New J. Phys.* **10** 075003

Howard M E, Beltran C, Anderson S, Tseung C, Sarkaria J N and Herman M G 2018 Investigating Dependencies of Relative Biological Effectiveness for Proton Therapy in Cancer Cells *Int. J. Part. Ther.* **4** 12–22

IAEA 2000 *IAEA Technical Report Series No. 398* (International Atomic Energy Agency (IAEA))

IAEA 2008 Relative Biological Effectiveness in Ion Beam Therapy *IAEA Tech. Reports* 1–165

ICRU 2011 Fundamental quantities and units for ionizing radiation (Revised) (ICRU Report 85) *Int. Comm. Radiat. Units Meas.*

ICRU 1983 Microdosimetry (ICRU Report 36) *Int. Comm. Radiat. Units Meas.*

ICRU 2007 Prescribing, recording, and reporting proton-beam therapy (ICRU Report 78) *Int. Comm. Radiat. Units Meas.*

Inaniwa T, Furukawa T, Kase Y, Matsufuji N, Toshito T, Matsumoto Y, Furusawa Y and Noda K 2010 Treatment planning for a scanned carbon beam with a modified microdosimetric kinetic model. *Phys. Med. Biol.* **55** 6721–37

Inaniwa T, Kanematsu N, Matsufuji N, Kanai T, Shirai T, Noda K, Tsuji H, Kamada T and Tsujii H 2015 Reformulation of a clinical-dose system for carbon-ion radiotherapy treatment planning at the National Institute of Radiological Sciences, Japan. *Phys. Med. Biol.* **60** 3271–86

Joiner M C and van der Kogel A 2009 *Basic clinical radiobiology* (Hodder Arnold)

Kanai T, Endo M, Minohara S, Miyahara N, Koyama-Ito H, Tomura H, Matsufuji N, Futami Y, Fukumura A, Hiraoka T, Furusawa Y, Ando K, Suzuki M, Soga F and Kawachi K 1999 Biophysical characteristics of HIMAC clinical irradiation system for heavy-ion radiation therapy *Int. J. Radiat. Oncol. Biol. Phys.* **44** 201–10

Kantemiris I, Karaiskos P, Papagiannis P and Angelopoulos A 2011 Dose and dose averaged LET comparison of ^{1}H, ^{4}He, ^{6}Li, ^{8}Be, ^{10}B, ^{12}C, ^{14}N, and ^{16}O ion beams forming a spread-out Bragg peak *Med. Phys.* **38** 6585–91

Karger C P and Peschke P 2018 RBE and related modeling in carbon-ion therapy *Phys. Med. Biol.* **63** 01TR02

Kase Y, Kanai T, Matsufuji N, Furusawa Y, Elsässer T and Scholz M 2008 Biophysical calculation of cell survival probabilities using amorphous track structure models for heavy-ion irradiation. *Phys. Med. Biol.* **53** 37–59

Kase Y, Kanai T, Matsumoto Y, Furusawa Y, Okamoto H, Asaba T, Sakama M and Shinoda H 2006 Microdosimetric measurements and estimation of human cell survival for heavy-ion beams *Radiat. Res.* **166** 629–38

Kelada O J and Carlson D J 2014 Molecular Imaging of Tumor Hypoxia with Positron Emission Tomography *Radiat. Res.* **181** 335–49

Kiefer J and Straaten H 1986 A model of ion track structure based on classical collision dynamics *Phys. Med. Biol.* **31** 1201–9

Koch C J and Evans S M 2015 Optimizing Hypoxia Detection and Treatment Strategies *Semin. Nucl. Med.* **45** 163–76

Kozłowska W S, Böhlen T T, Cuccagna C, Ferrari A, Fracchiolla F, Magro G, Mairani A, Schwarz M, Vlachoudis V and Georg D 2019 FLUKA particle therapy tool for Monte Carlo independent calculation of scanned proton and carbon ion beam therapy *Phys. Med. Biol.* **64** 075012

Krämer M and Scholz M 2000 Treatment planning for heavy-ion radiotherapy: calculation and optimization of biologically effective dose *Phys. Med. Biol.* **45** 3319–30

Lederman M 1981 The early history of radiotherapy: 1895-1939 *Int. J. Radiat. Oncol. Biol. Phys.* **7** 639–48

Leeuwen C M Van, Oei A L, Crezee J, Bel A, Franken N A P, Stalpers L J A and Kok H P 2018 The alfa and beta of tumours: a review of parameters of the linear-quadratic model , derived from clinical radiotherapy studies *Radiat. Oncol.* **13** 96

Leo W R 2012 *Techniques for nuclear and particle physics experiments: a how-to approach* (Springer Science & Business Media)

Liamsuwan T, Hultqvist M, Lindborg L, Uehara S and Nikjoo H 2014 Microdosimetry of proton and carbon ions *Med. Phys.* **41** 081721

Lin Z, Mechalakos J, Nehmeh S, Schoder H, Lee N, Humm J and Ling C C 2008 The Influence of Changes in Tumor Hypoxia on Dose-Painting Treatment Plans Based on ^{18}F-FMISO Positron Emission Tomography *Int. J. Radiat. Oncol. Biol. Phys.* **70** 1219–28

Lühr A, von Neubeck C, Helmbrecht S, Baumann M, Enghardt W and Krause M 2017 Modeling in vivo relative biological effectiveness in particle therapy for clinically relevant endpoints *Acta Oncol. (Madr).* **56** 1392–8

Lühr A, Toftegaard J, Kantemiris I, Hansen D C and Bassler N 2012 Stopping power for particle therapy: the generic library libdEdx and clinically relevant stopping-power ratios for light ions. *Int. J. Radiat. Biol.* **88** 209–12

Mairani A, Böhlen T T, Schiavi A, Tessonnier T, Molinelli S, Brons S, Battistoni G, Parodi K and Patera V 2013 A Monte Carlo-based treatment planning tool for proton therapy *Phys. Med. Biol.* **58** 2471–90

Mairani A, Brons S, Cerutti F, Fassò A, Ferrari A, Krämer M, Parodi K, Scholz M and Sommerer F 2010 The FLUKA Monte Carlo code coupled with the local effect model for biological calculations in carbon ion therapy *Phys. Med. Biol.* **55** 4273–89

Mairani A, Magro G, Tessonnier T, Böhlen T T, Molinelli S, Ferrari A, Parodi K, Debus J and Haberer T 2017 Optimizing the modified microdosimetric kinetic model input parameters for proton and ^{4}He ion beam therapy application *Phys. Med. Biol.* **62** N244–56

Malinen E and Søvik Å 2015 Dose or LET painting - What is optimal in particle therapy of hypoxic tumors? *Acta Oncol. (Madr).* **54** 1614–22

McMahon S J 2019 The linear quadratic model: Usage, interpretation and challenges *Phys. Med. Biol.* **64** 01TR01

McNamara A, Willers H and Paganetti H 2019 Proton Therapy special feature : Review Article Modelling variable proton relative biological effectiveness for treatment planning *Br J Radiol* **92** 20190334

MD Anderson Cancer Center 2019 LET Optimized IMPT in Treating Pediatric Patients With Ependymoma, ClinicalTrials.gov Identifier: NCT03750513 *ClinicalTrials.gov*

Molinelli S, Magro G, Mairani A, Matsufuji N, Kanematsu N, Inaniwa T, Mirandola A, Russo S, Mastella E, Hasegawa A, Tsuji H, Yamada S, Vischioni B, Vitolo V, Ferrari A, Ciocca M, Kamada T, Tsujii H, Orecchia R and Fossati P 2016 Dose prescription in carbon ion radiotherapy: How to compare two different RBE-weighted dose calculation systems *Radiother. Oncol.* **120** 307–12

Newhauser W D and Zhang R 2015 The physics of proton therapy *Phys. Med. Biol.* **60** R155–209

Paganetti H 2015 Relating proton treatments to photon treatments via the relative biological effectiveness - Should we revise current clinical practice? *Int. J. Radiat. Oncol. Biol. Phys.* **91** 892–4

Paganetti H 2014 Relative biological effectiveness (RBE) values for proton beam therapy. Variations as a function of biological endpoint, dose, and linear energy transfer. *Phys. Med. Biol.* **59** R419-72

Paganetti H, Blakely E, Carabe-Fernandez A, Carlson D J, Das I J, Dong L, Grosshans D, Held K D, Mohan R, Moiseenko V, Niemierko A, Stewart R D and Willers H 2019 Report of the AAPM TG-256 on the relative biological effectiveness of proton beams in radiation therapy *Med. Phys.* **46** e53–78

Parodi K, Mairani A, Brons S, Hasch B G, Sommerer F, Naumann J, Jäkel O, Haberer T and Debus J 2012 Monte Carlo simulations to support start-up and treatment planning of scanned proton and carbon ion therapy at a synchrotron-based facility *Phys. Med. Biol.* **57** 3759–84

Peeler C R, Mirkovic D, Titt U, Blanchard P, Gunther J R, Mahajan A, Mohan R and Grosshans D R 2016 Clinical evidence of variable proton biological effectiveness in pediatric patients treated for ependymoma *Radiother. Oncol.* **121** 395–401

Prise K M, Folkard M, Davies S and Michael B D 1990 The irradiation of V79 mammalian cells by protons with energies below 2 MeV. Part II. Measurement of oxygen enhancement ratios and DNA damage *Int. J. Radiat. Biol.* **58** 261–77

PTCOG 2019 Particle therapy facilities in operation Online: https://www.ptcog.ch/index.php/facilities-in-operation

Quaresma M, Coleman M P and Rachet B 2015 40-year trends in an index of survival for all cancers combined and survival adjusted for age and sex for each cancer in England and Wales, 1971-2011: A population-based study *Lancet* **385** 1206–18

Rath A K and Sahoo N 2016 *Particle radiotherapy: Emerging technology for treatment of cancer* (Springer)

RaySearch 2019 Press release Online: https://mb.cision.com/Main/1102/2880766/1089844.pdf

Remmes N B, Herman M G and Kruse J J 2012 Optimizing normal tissue sparing in ion therapy using calculated isoeffective dose for ion selection *Int. J. Radiat. Oncol. Biol. Phys.* **83** 756–62

Röntgen W C 1896 On a new kind of rays *Science* **3** 227–31

Rørvik E, Fjæra L F, Dahle T J, Dale J E, Engeseth G M, Camilla Stokkevåg H, Thörnqvist S and Ytre-Hauge and K S 2018 Exploration and application of phenomenological RBE models for proton therapy *Phys. Med. Biol.* **63** 185013

Rørvik E, Thornqvist S, Stokkevag C H, Dahle T J, Fjæra L F and Ytre-Hauge K S 2017 A phenomenological biological dose model for proton therapy based on linear energy transfer spectra *Med. Phys.* **44** 2586–94

Rosenfeld A B 2016 Novel detectors for silicon based microdosimetry, their concepts and applications *Nucl. Instruments Methods Phys. Res. Sect. A Accel. Spectrometers, Detect. Assoc. Equip.* **809** 156–70

Rykkelid A M 2017 *Method for in vitro Cell Irradiation with Low Energy Protons* (Master thesis, University of Oslo) Online: https://www.duo.uio.no/handle/10852/61281

Saager M, Peschke P, Welzel T, Huang L, Brons S, Grün R, Scholz M, Debus J and Karger C P 2018 Late normal tissue response in the rat spinal cord after carbon ion irradiation *Radiat. Oncol.* **13** 1–9

Schardt D, Elsässer T and Schulz-Ertner D 2010 Heavy-ion tumor therapy: Physical and radiobiological benefits *Rev. Mod. Phys.* **82** 383–425

Scholz M 2003 Effects of ion radiation on cells and tissues *Radiation effects on plymers for biological use* (Springer) pp 95–155

Scholz M and Elsässer T 2007 Biophysical models in ion beam radiotherapy *Adv. Sp. Res.* **40** 1381–91

Scholz M, Kellerer A M, Kraft-Weyrather W and Kraft G 1997 Computation of cell survival in heavy ion beams for therapy: The model and its approximation *Radiat. Environ. Biophys.* **36** 59–66

Scholz M and Kraft G 1996 Track structure and the calculation of biological effects of heavy charged particles *Adv. Sp. Res.* **18** 5–14

Schuemann J, Giantsoudi D, Grassberger C, Moteabbed M, Min C H and Paganetti H 2015 Assessing the Clinical Impact of Approximations in Analytical Dose Calculations for Proton Therapy *Int. J. Radiat. Oncol. Biol. Phys.* **92** 1157–64

Scifoni E, Tinganelli W, Weyrather W K, Durante M, Maier A and Krämer M 2013 Including oxygen enhancement ratio in ion beam treatment planning: Model implementation and experimental verification *Phys. Med. Biol.* **58** 3871–95

Silvoniemi A 2018 *Novel aspects for methodology and utilization of PET/CT imaging in head and neck cancer* (Academic dissertation, University of Turku) Online: https://www.utupub.fi/handle/10024/144772

Solov'yov A V. 2017 *Nanoscale insights into ion-beam cancer therapy* (Springer)

Sørensen B S, Bassler N, Nielsen S, Horsman M R, Grzanka L, Spejlborg H, Swakoń J, Olko P and Overgaard J 2017 Relative biological effectiveness (RBE) and distal edge effects of proton radiation on early damage in vivo *Acta Oncol. (Madr).* **56** 1387–91

Strigari L, Torriani F, Manganaro L, Inaniwa T, Dalmasso F, Cirio R and Attili A 2018 Tumour control in ion beam radiotherapy with different ions in the presence of hypoxia: An oxygen enhancement ratio model based on the microdosimetric kinetic model *Phys. Med. Biol.* **63** 065012

Tessonnier T, Mairani A, Cappucci F, Mirandola A, Vilches Freixas G, Molinelli S, Donetti M and Ciocca M 2014 Development and application of tools for Monte Carlo based simulations in a particle beam radiotherapy facility *Appl. Radiat. Isot.* **83** 155–8

Tinganelli W, Durante M, Hirayama R, Krämer M, Maier A, Kraft-Weyrather W, Furusawa Y, Friedrich T and Scifoni E 2015 Kill-painting of hypoxic tumours in charged particle therapy *Sci. Rep.* **5** 1–13

Tormodsrud V H 2019 *Relative Biologic Effectiveness and Linear Energy Transfer effects of low energy proton irradiations for T98G human glioblastoma cells* (Master thesis, University of Oslo) Online: https://www.duo.uio.no/handle/10852/70379

Underwood T S A, Grassberger C, Bass R, MacDonald S M, Meyersohn N M, Yeap B Y, Jimenez R B and Paganetti H 2018 Asymptomatic Late-phase Radiographic Changes Among Chest-Wall Patients Are Associated With a Proton RBE Exceeding 1.1 *Int. J. Radiat. Oncol. Biol. Phys.* **101** 809–19

Weber U and Kraft G 2009 Comparison of Carbon Ions Versus Protons *Cancer J.* **15** 325–32

Weisstein E W 2003 Circle-Circle Intersection *MathWorld--A Wolfram Web Resour.* Online: http://mathworld.wolfram.com/Circle-CircleIntersection.html

Welsh L, Panek R, Riddell A, Wong K, Leach M O, Tavassoli M, Rahman D, Schmidt M, Hurley T, Grove L, Richards T, Koh D M, Nutting C, Harrington K, Newbold K and Bhide S 2017 Blood transfusion during radical chemo-radiotherapy does not reduce tumour hypoxia in squamous cell cancer of the head and neck *Br. J. Cancer* **116** 28–35

Wenzl T and Wilkens J J 2011 Modelling of the oxygen enhancement ratio for ion beam radiation therapy *Phys. Med. Biol.* **56** 3251–68

WHO 2018 World health organization cancer statistics Online: https://www.who.int/cancer/en/

Wilkens J J and Oelfke U 2004 Three-dimensional LET calculations for treatment planning of proton therapy. *Z. Med. Phys.* **14** 41–6

Willers H, Allen A, Grosshans D, McMahon S J, von Neubeck C, Wiese C and Vikram B 2018 Toward A variable RBE for proton beam therapy *Radiother. Oncol.* **128** 68–75

Wilson R R 1946 Radiological use of fast protons *Radiology* **47** 487–91

Yepes P, Adair A, Frank S J, Grosshans D R, Liao Z, Liu A, Mirkovic D, Poenisch F, Titt U, Wang Q and Mohan R 2019 Fixed- versus Variable-RBE Computations for Intensity Modulated Proton Therapy *Adv. Radiat. Oncol.* **4** 156–67

Graphic design: Communication Division, UiB / Print: Skipnes Kommunikasjon AS

uib.no

ISBN: 9788230861196 (print)
9788230850305 (PDF)